ANL-7799

CHEMICAL ENGINEERING DIVISION
FUEL CYCLE TECHNOLOGY QUARTERLY REPORT

January, February, March 1971

D. S. Webster, A. A. Jonke, G. J. Bernstein,
N. M. Levitz, R. D. Pierce,
M. J. Steindler, and R. C. Vogel

ARGONNE NATIONAL LABORATORY, ARGONNE, ILLINOIS

Printed in the United States of America
Available from
National Technical Information Service
U.S. Department of Commerce
5285 Port Royal Road
Springfield, Virginia 22151
Price: Printed Copy $3.00; Microfiche $0.95

ANL-7799
Chemical Separations Processes
for Plutonium and Uranium

ARGONNE NATIONAL LABORATORY
9700 South Cass Avenue
Argonne, Illinois 60439

CHEMICAL ENGINEERING DIVISION
FUEL CYCLE TECHNOLOGY QUARTERLY REPORT

January, February, March 1971

by

D. S. Webster, A. A. Jonke, G. J. Bernstein,
N. M. Levitz, R. D. Pierce,
M. J. Steindler, and R. C. Vogel

July 1971

Previous reports in this series

ANL-7735, April, May, June 1970
ANL-7755, July, August, September 1970
ANL-7767, October, November, December 1970

TABLE OF CONTENTS

LIST OF FIGURES

LIST OF TABLES

FUEL CYCLE TECHNOLOGY QUARTERLY REPORT

January, February, March 1971

by

D. S. Webster, A. A. Jonke, G. J. Bernstein
N. M. Levitz, R. D. Pierce,
M. J. Steindler, and R. C. Vogel

ABSTRACT

During the period January through March, 1971, work was done in the following areas: (1) further development of a liquid-metal head-end process for LMFBR fuel by study of the reduction of declad fuel oxide, (2) investigation of a procedure for separating stainless steel cladding from fuel oxide by melting the cladding, (3) additional laboratory-scale work to develop a fluid-bed process for the conversion of uranyl nitrate and plutonium nitrate in nitric acid solutions to an oxide form (UO_2-PuO_2) suitable for the fabrication of fuel shapes for LMFBR fuel, (4) additional development of X-ray diffraction spectrometry as an in-line analytical method for determining the Pu/U ratio of oxide fuels during fabrication, (5) continued investigation of the performance characteristics of a centrifugal contactor for the plutonium isolation steps in the solvent extraction of LMFBR fuels, and (6) study of electrode reactions and process parameters that affect the electrolytic reduction and reoxidation of plutonium in the Purex process.

SUMMARY

I. Liquid Metal Decladding of Reactor Fuel

Head-end processing of LMFBR fuel will include fuel-subassembly handling, removal of stainless steel cladding and subassembly hardware from the fuel, removal of iodine and gases from the fuel, and feeding of fuel to a nitric acid dissolution step for subsequent aqueous processing. Early LMFBR fuel elements will consist of mixed uranium and plutonium oxides jacketed in stainless steel cladding. Two decladding procedures are being studied:

1) Dissolution of stainless steel components by submerging most of the fuel subassembly in molten zinc at 800°C, separation of the zinc-stainless steel solution from the unaffected oxide fuel, chemical reduction of the uranium-plutonium oxide to metal by contacting it with a molten metal-salt system, and subsequently feeding the uranium and plutonium to an acid-dissolution step. The principal attraction of this procedure is the complete containment of volatile fission products offered: iodine is retained as iodide in a cover salt, and tritium, xenon, and krypton are collected at high concentrations in argon cover gas.

2) Melting of stainless steel cladding and draining it away from the fuel (followed by feeding of the fuel oxide to a voloxidation or acid dissolution step).

Engineering Development of Zinc Decladding

Reduction of UO_2 Pellets. The fuel reduction step that follows decladding with molten zinc (1) liberates iodine, (2) allows the collection of iodine and the fission product gases, and (3) converts the uranium and plutonium oxides to a liquid metal solution for ease of handling. Although a Mg-Cu-Ca/$CaCl_2$-CaF_2 reduction system developed for the Salt Transport Process would perform well, it would be desirable to substitute zinc for copper in the present application since the solvent metals could then be removed from the fuel by evaporation. Testing of two different Zn-Mg-Ca systems has been continued: (1) an alloy with a high zinc-to-magnesium ratio (atomic ratio = 2 1/3) for use when it is desired to dissolve both reduced uranium and reduced plutonium in the solvent metal and (2) an alloy with a low zinc-to-magnesium ratio (atomic ratio = 0.25) for use when only reduced plutonium is to be dissolved in the solvent metal. Both alloys were evaluated with and without added calcium for the reduction of sintered UO_2 pellets. The salt used was 80 mol % $CaCl_2$-20 mol % CaF_2. Good reductions were obtained with systems that included calcium; in the absence of calcium, reduction rates were low. A few runs are under way to select the most favorable composition of the $CaCl_2$-CaF_2 reduction salt and to establish the limiting loading of the reduction salt with CaO reaction product. Good reductions of the UO_2 were obtained even when the CaF_2 content of the salt was zero. However, the metal and salt phases separate better when CaF_2 is present. In runs producing high CaO loadings in the salt, reduction was faster with the low-zinc Zn-Mg-Ca alloy than with the high-zinc alloy. This difference is attributed to better fuel-salt contacting with the lighter low-zinc alloy--this alloy floats on the salt, and the salt and fuel are in intimate contact near the impellor (this reduction is believed to be a salt-phase reaction).

Process Demonstration Experiments

Experimental apparatus for the demonstration of the zinc-decladding process with 100 g of irradiated fuel has been assembled and tested outside the shielded hot cell. The apparatus will next be moved into the shielded cell. Two irradiated UO_2-20 mol % PuO_2 fuel elements have been obtained for the hot experiments. This fuel, clad with type 316 stainless steel, was irradiated to about 3.6 at. % burnup at a maximum peak linear power of 13.8 kW/ft.

Melt Decladding

Investigations continued on the separation of fuel oxide from stainless steel cladding by melting the cladding and draining it away from the fuel. The feasibility of the procedure depends on the oxide surface being sufficiently exposed so that in the following step the oxide can be completely separated from the steel by either dissolution in acid or voloxidation.

A series of experiments was completed to observe the degree to which steel would flow away from a bundle of simulated fuel elements that were either supported on an incline during heating or tilted after heating to ~1550 to 1600°C. A slope of 15 or 20° resulted in excessive quantities of oxide particles accompanying the steel; an angle of 10° appears to be preferable.

The density of the sintered pellets influenced the degree of wetting of oxide by stainless steel. Pellets of >93% of theoretical density were wet less than pellets of 87% of theoretical density. Pending the results of conceptual-design studies, no further experiments are planned on inclined-surface melt decladding.

Additional experiments are planned to investigate lowering a simulated fuel subassembly into a heated zone to melt the cladding. Molten steel and released fuel will fall to a cold surface, where the metal will solidify.

II. Continuous Conversion of U/Pu Nitrates to Oxides

A continuous fluidized-bed denitration process is under development for converting uranyl nitrate-plutonium nitrate solutions to mixed oxides suitable for the fabrication of fuel shapes.

Further electron microprobe examination of UO_2-20% PuO_2 pellets was carried out in the laboratory. The pellets, prepared earlier from powder formed by drop denitration of a U/Pu nitrate solution followed by hydrogen reduction, showed good distribution of the plutonium oxide in the uranium oxide matrix. Complete scans across a diameter revealed some point-to-point variation of the uranium-to-plutonium ratio, but no evidence of plutonium segregation.

Knowledge of the cosolubility of uranyl nitrate hexahydrate (UNH) and plutonium nitrate in dilute nitric acid solutions is pertinent to the selection of the feed solution composition for the fluid-bed denitration process. The crystallization temperatures of ten mixed actinide solutions and several uranyl nitrate solutions in the range 1-2M (U+Pu) have been measured.

Crystallization temperatures increased almost linearly with increasing acid concentration in the range 2-4M for the mixed actinide solutions. The same effect was observed for uranyl nitrate solutions, although the increases in crystallization temperature with increasing acidity were slightly greater. At nitric acid concentrations higher than 4M, a given change in nitric acid concentration had less effect on crystallization temperature than at lower acidities.

Substitution of plutonium for some of the uranium in the nitrate solutions lowered the crystallization temperature, e.g., at a fixed nitric acid concentration (3.4M) and a fixed concentration (1.4M) of uranium or uranium plus plutonium, the crystallization temperature decreased from 12.8°C for uranyl nitrate alone to 1.5°C for a solution in which the plutonium fraction was 0.5. The data indicate that with 2.0M excess nitric acid, relatively concentrated feed solutions, on the order of 1.8M (U+Pu), can be employed at room temperature in fluidized-bed experiments without concern about crystallization.

Installation work to prepare the denitration pilot plant for work with U/Pu materials is nearly complete.

III. In-Line Analysis in Fuel Fabrication

The analytical requirements of fuel fabrication operations are a major factor in the cost of fabricating LMFBR fuel. The large number of pellets to be processed coupled with the rigorous specifications and quality control procedures make automated sample handling and analyses an economic necessity. The present program is designed to develop rapid, precise, and accurate in-line analytical methods applicable to the fabrication of oxidic LMFBR fuels. In the evaluation of analytical methods, the specifications of preirradiation properties for the Fast Flux Test Facility (FFTF) project have been selected as starting criteria.

Emphasis has been placed on the development of X-ray fluorescence analysis to determine Pu/U ratio, using urania and thoria as stand-ins for fuel material. New counting equipment manufactured by Philips Electronic Instruments, Inc., has been put into operation. Because of high counting rates obtained for uranium and thorium with this equipment, significant corrections for dead time and coincidence were required. Calibration of the detector and counter has been completed in situ, utilizing nickel absorbers, and a correction relationship has been calculated over the range 900 to 90,000 cps.

In work to establish the relationship between line intensity and composition, four sets of data were obtained for powder mixtures of 10, 15, 20, 25, and 30 wt % UO_2 in ThO_2. The relative standard deviations for each concentration range were 0.28-0.37% for uranium and 0.78-2.2% for thorium. Other experiments with sintered pellets formed from powders containing 10, 20, and 30% urania in thoria show relative standard deviations of 0.65 and 0.03% for the fluorescence measurements of uranium and thorium, respectively.

The possibility that impurity elements will interfere in the X-ray fluorescence analysis of uranium-plutonium oxide fuel materials for FFTF has been reviewed. Only strontium, if present in concentrations greater than 100 ppm, could interfere with analysis of fuel that meets FFTF specifications. For future LMFBR fuels of different compositions, the elements Pa, Np, Am, and Cm in plutonium will have to be considered as potential interfering elements.

Progress is also reported on improving the precision of the method by controlling sample presentation methods.

IV. Adaptation of Centrifugal Contactors in LMFBR Fuel Processing

The performance characteristics of centrifugal contactors suitable for use for plutonium purification in the Purex-type solvent extraction of LMFBR fuel material are being investigated. A contactor design is being studied in which the diameter of the unit is limited to geometrically favorable dimensions in order to minimize the criticality hazards associated with the high plutonium concentrations in the process streams.

A stainless steel contactor based on the design of the large centrifugal contactor in use at Savannah River has been fabricated. The hollow

rotor (4-in. ID by 15 in. long) was designed to operate at speeds up to 3600 rpm. Since a high level of dynamic stability is required for good mechanical performance, dynamic testing was carried out both on the rotor components and on the finished rotor after assembly. Final testing of the empty contactor was done after the unit was mounted in the contactor test facility. Vibration at rotor speeds up to 4000 rpm was very low, indicating that the degree of precision exercised in fabrication was sufficient to meet the rigid design specifications for this developmental unit.

Preliminary testing of the contactor was carried out to evaluate hydraulic and mechanical performance. In initial runs, 0.03M HNO_3 was employed as the aqueous phase and Ultrasene (refined kerosene) as the organic phase. Some flow surging was noted during these runs. Surging can reduce separating capacity since variations in flow rate through the rotor cause shifting and widening of the emulsion band at the top of the rotor (where the aqueous and organic phases are separated), leading to excessive entrainment of one phase in the other. Surging was essentially eliminated by increasing the size of the baffles in the mixing chamber. With an aqueous-to-organic (A/O) flow ratio of 1:1, the separating capacity with less than 1 vol % entrainment in the effluent streams ranged from 10 gpm (total for both phases) at 2000 rpm to 18 gpm at 3500 rpm.

Additional tests were made with an aqueous phase of 0.5M HNO_3 and an organic phase of 15% tributyl phosphate in Ultrasene. A recurrence of flow surging was eliminated by installing additional baffles in the mixing chamber. Separating capacity at an A/O ratio of 1:1 ranged from 5.6 gpm at 2000 rpm to 10 gpm at 3500 rpm. The reduced capacity, as compared with the capacity obtained with the previous acid-Ultrasene system, is attributed to the formation of mixtures more difficult to separate.

V. Electrolytic Reduction and Reoxidation of Plutonium in Purex Processes

Electrolytic reduction of plutonium is being developed as a substitute for chemical reductants used in the Purex process. The pertinent electrode reactions in the literature have been reviewed and scale-up implications have been considered. The presence of uranyl ion may effect the reduction of plutonium. A scheme for integrating flow-through electrolytic cells into a bank of centrifugal contactors has been developed and tested by an idealized material balance calculation.

A major objective of this investigation has been to assure an adequate reduction rate under process conditions. Cell design and process parameters that affect the reduction rate in a continuous electrolytic cell have been identified: the reduction rate is mass transport-related and can be described over the flow range of $100 < Re < 2000$ by $Nu = A\, Re^{1/2}\, Sc^{1/3}$, where Re is the Reynolds number, Nu the Nusselt number, Sc the Schmidt number, and A a proportionality constant. The inherent assumptions in this equation are discussed, and modifications for extending the range of applicability are suggested. From these considerations, an equation describing the effectiveness of an electrolytic cell has been developed. Effectiveness is linked to the residence time in the cell required to reach a desired level of reduction.

The pressure drop across a schematically designed cell is calculated. From a comparison of the equations for pressure drop and effectiveness, a set of rules for designing cells is derived. High reduction rates are achieved in cells with (1) a high ratio of electrode surface area to cell volume, (2) an electrode whose characteristic dimension is small, and (3) high flow velocity of the solution. The first of these parameters has the most effect in increasing reduction rates, the second is less effective, and the third has a small effect. A cell suitable for plutonium reduction and reoxidation in a Purex application would be slab-shaped, 45 cm long, 20 cm wide, and 10 to 15 cm thick.

I. LIQUID-METAL DECLADDING OF REACTOR FUELS

(R. D. Pierce)

Liquid-metal decladding processes under development at Argonne appear to provide relatively simple and inexpensive techniques for solving formidable head-end processing problems related to the high burnups, short cooling times, and residual sodium of irradiated LMFBR fuels.

Early LMFBR fuel elements will consist of mixed uranium and plutonium oxides jacketed in stainless steel tubes. After irradiation, these fuels may be allowed to decay for as little as 30 days. The localized heat emission of LMFBR fuels is very high, creating heat-dissipation problems during handling and processing operations.

High concentrations of radioactive iodine (especially ^{131}I), xenon, and krypton in spent LMFBR fuel will present serious problems in handling and disposing of the waste-gas effluent from reprocessing operations. To avoid excessive emissions of highly radioactive isotopes such as ^{131}I to the environment, head-end operations must be performed in a sealed cell, and fission gases must be contained efficiently. If possible, the volatile elements should be removed from the fuel material prior to the nitric acid dissolution step of aqueous fuel processing.

If sodium is present in failed fuel elements, it too could present cleaning and fuel-dissolution problems since sodium can react explosively with nitric acid. In addition, the high plutonium content of LMFBR fuel presents criticality problems.

In one scheme for liquid-metal decladding, cladding is removed by immersing all of the fuel region of a discharged fuel subassembly in a pool of molten zinc having a molten-salt cover layer. (Probably, the bottom of the fuel subassembly would be cropped prior to immersion.)

The zinc dissolves the stainless steel components (i.e., the subassembly supporting members and the cladding), but does not react with the fuel oxides. The resulting zinc solution is then removed from the decladding vessel to separate it from the fuel oxides. The fuel oxides are next reduced to metal with Mg-Zn-Ca in the presence of a salt phase, and the uranium and plutonium are removed from the decladding vessel in a liquid-metal solution. The reduced fuel is dissolved in nitric acid for further purification. During the decladding and reduction steps, all of the sodium, iodine, and fission-product gases are removed from the fuel.

Advantages of liquid-metal decladding include (1) efficient removal of iodine and other volatile fission products, (2) relative ease of dissipation of fission-product heat, (3) elimination of the requirement for separate sodium-removal steps, (4) discharge of all process waste streams (except Xe and Kr) as solids having good heat-transfer properties, (5) collection of xenon and krypton in an inert cover-gas mixture (containing ~50% Xe plus Kr) of small enough volume to allow storage in gas cylinders, and (6) process simplicity and flexibility.

The principal disadvantages of liquid-metal decladding are a lack of industrial experience in the use of refractory metals and graphite as materials of construction, and the need to dispose of large quantities of reagent zinc as waste. Although refractory metals and graphite are compatible with liquid zinc and molten salts and although equipment fabricated of these materials have long lives, their cost is a significant portion of the processing cost. About 12 ft^3 of zinc and 20 ft^3 of salt are used for each ton of fuel processed. However, these solids are good waste forms, and the reagent and waste-disposal costs are not large. As an alternative to storage, these reagents may be recovered by a vacuum-vaporization process for recycle.

Another scheme for liquid-metal decladding utilizes direct melting of the stainless steel cladding and subassembly supporting members. A major portion of the molten steel can be separated from the fuel and cast into a waste ingot; the steel still associated with the fuel can be charged with the fuel to either an acid dissolution step or a voloxidation step to complete the separation of steel from fuel. Melt decladding avoids mechanical dismantling of the fuel, allows liberated fission gases to be collected in a compact form, evaporates residual sodium from the fuel, provides a compact waste, and adds no extraneous metal to the fuel before it is fed to the acid dissolution step. The major difficulties of the step are high temperature (>1450°C), relatively poor separation of steel and oxide, difficulties in handling the declad fuel, and low removal of iodine from the fuel.

A. Engineering Development of Zinc Decladding (I. O. Winsch, T. F. Cannon, J. J. Stockbar)

The first step in a procedure proposed for liquid-metal decladding is to dissolve stainless steel cladding by immersing fuel subassemblies in molten zinc (contained in a tungsten decladding vessel at 800°C). The zinc-steel solution thereby produced is transferred out of the vessel away from the fuel. A $Mg-Zn-Ca/CaCl_2-CaF_2$ system is added to the fuel oxide in the decladding vessel and heated.

By contacting the oxide fuel with the molten metal/salt system, the fuel oxide is next reduced to metal and dissolved in the reduction alloy. The salt becomes a waste stream, and the metal phase containing the reduced fuel, which is the head-end product, may be pressured-siphoned out of the reaction vessel. The product solution may be further concentrated by evaporating away all or part of the solvent alloy prior to dissolution of the metallic fuel in nitric acid for aqueous solvent extraction processing. In the reduction procedure, all iodine would be released and collected in the waste salt and all gaseous fission products would be released in the sealed decladding furnace and collected for storage with minimum dilution by other gases. The latter are advantages of liquid-metal decladding.

Two reduction schemes are proposed: One employs a high-zinc reduction alloy and the liquid metal product contains both plutonium and uranium; the other employs a low-zinc reduction alloy, and the products are precipitated metallic uranium and a solution containing plutonium. In the latter scheme, the uranium is dissolved in another

metal alloy after the plutonium-bearing solution is transferred out of the reaction vessel. Flowsheets for the two cases are presented as Fig. I-1 and I-2.

A few reduction runs were made to determine (1) whether calcium was required with the magnesium and zinc in the reduction alloy to obtain adequate reduction rates with high-fired oxide pellets, (2) the practical loading limit for CaO in the waste reduction salt, and (3) the minimum concentration of CaF_2 in the salt fed to the reduction step to obtain good metal-salt phase separations.

1. Reduction of UO_2 Pellets

In the reduction step that follows zinc decladding in the proposed liquid-metal head-end process, declad oxide fuel is contacted with a liquid salt and a molten-metal alloy containing a reductant. With adequate stirring of the fuel oxide, salt, and metal phases, the UO_2 and PuO_2 are converted to metal, and the reduced plutonium is dissolved in the liquid-metal solution. The composition and quantity of the reduction alloy determine whether the reduced uranium is dissolved in the liquid-metal solution, precipitated, or partially dissolved.

A salt-metal system which was successfully developed for reduction of UO_2 and PuO_2 for the Salt Transport Process consists of calcium dissolved in Mg-42 at. % Cu and $CaCl_2$-20 mol % CaF_2 salt (ANL-7735, pp. 21-25).

As an alternative to Mg-Cu alloys, two Zn-Mg alloys (which can be recovered by evaporation and recycled) are being evaluated for the reduction system in a limited number of runs. The alloys under investigation are (1) 70 at. % Zn-30 at. % Mg, which is rich in zinc and yields a product solution containing reduced uranium and plutonium and (2) 80 at. % Mg-20 at. % Zn, which is low in zinc and yields a product solution containing only plutonium. Similar alloys were used successfully to reduce unfired U_3O_8 in the Skull Reclamation Process for EBR-II.[1]

Runs were made with and without calcium added to these alloys. Sintered UO_2 pellets were reduced at 800°C. Previous experience had shown that UO_2 is more difficult to reduce than either PuO_2 or $(Pu,U)O_2$ in these metal-salt systems.[2]

Data for all runs are tabulated in Table I-1. Four runs were made with calcium absent from the metal phase. Three runs that used the Mg-Zn/$MgCl_2$-$CaCl_2$-CaF_2 reduction systems developed for the Skull Reclamation Process[1] (runs Mg-Zn-2, -3, and -7) resulted in slow reductions that were incomplete after 5 hr. An extremely poor reduction was obtained using a Mg-Zn/$CaCl_2$-CaF_2 system (run Mg-Zn-6). Where magnesium is the reducing agent, $MgCl_2$ has proved to be an important salt ingredient for the reduction of UO_2.[3] No further runs with calcium absent are planned. With calcium present, both the high-zinc system (runs Mg-Zn-5 and -8) and the low-zinc system (runs Mg-Zn-4 and -9) gave excellent reductions at a final salt composition of 13 mol % CaO-70 mol %

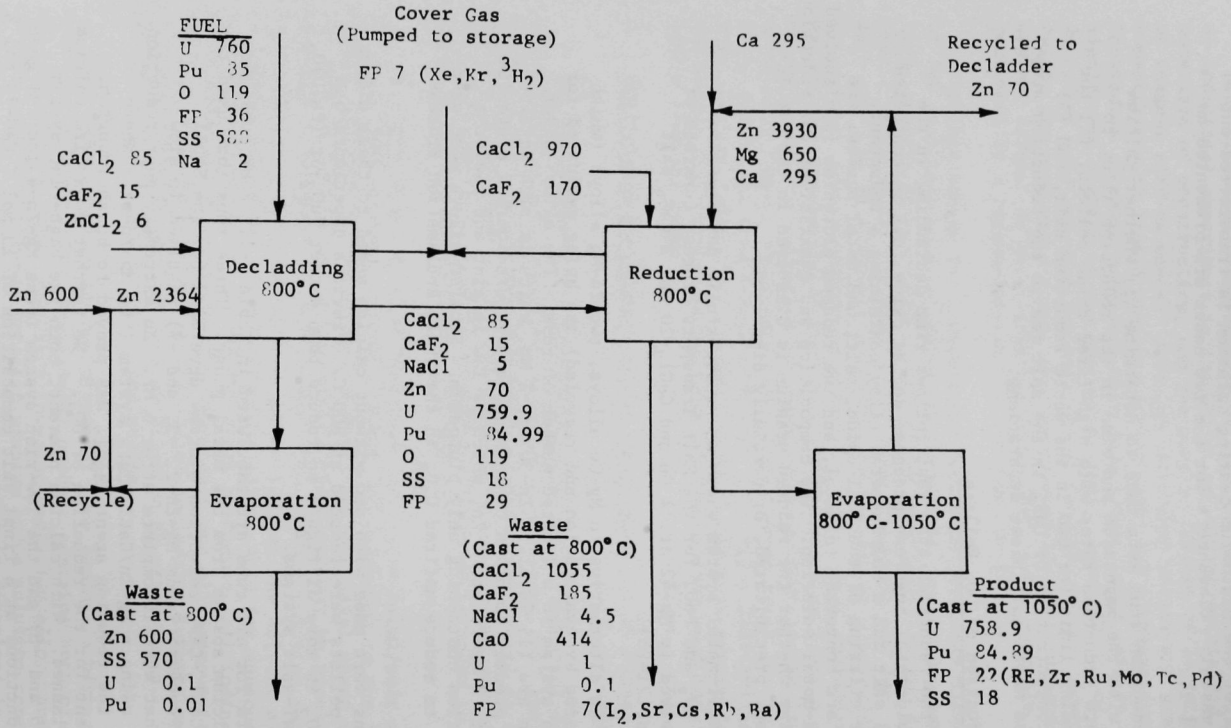

Fig. I-1. Head-end Molten Metal-Salt Process Employing a High-Zinc Reduction Alloy

Product: Combined U and Pu
Basis: 1 metric ton of fuel
Quantities in kilograms

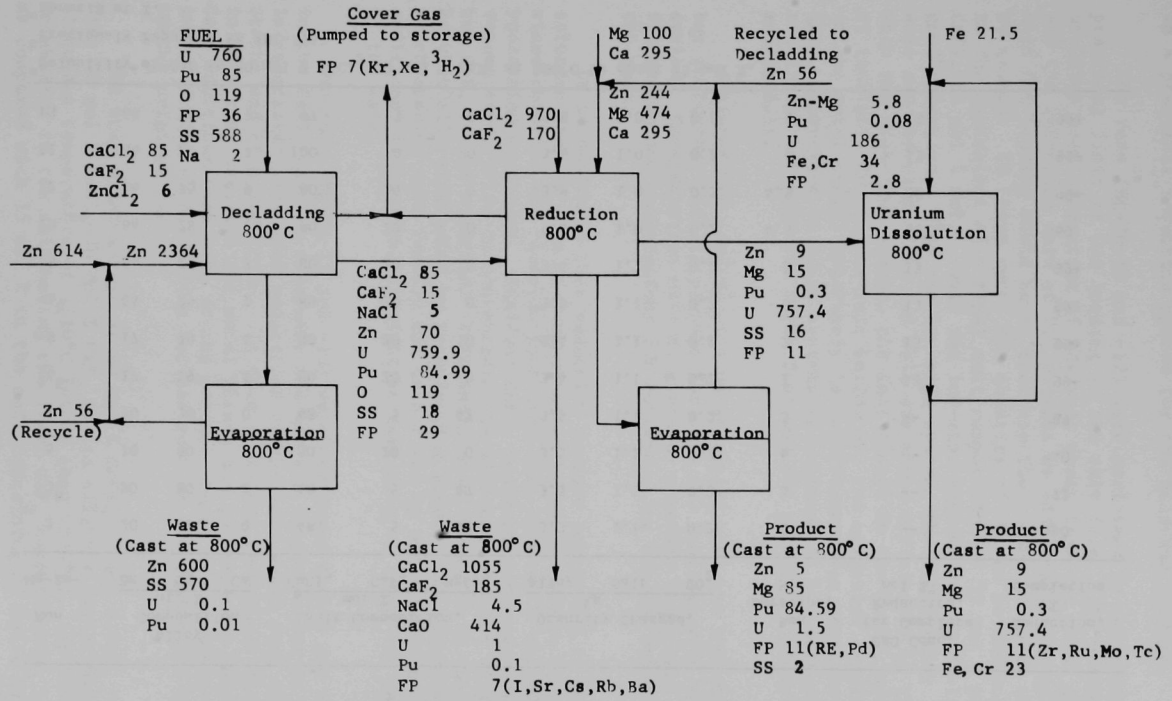

Fig. I-2. Head-end Molten Metal-Salt Process Employing a Low-Zinc Reduction Alloy

Products: Separate U- and Pu-bearing alloys
Basis: 1 metric ton of fuel
Quantities in kilograms

TABLE I-1. UO_2 Reduction Runs

Crucible: Baffled, tungsten, 5 1/2-in. ID
Agitator: 3-in. dia, 1 1/4-in.-wide blade, pitched 30° from the horizontal, deflecting downward, 1/2 in. above the bottom of the vessel
Sintered UO_2 Pellets: 0.21-in. dia; 0.25 in. long
Temperature: 800°C
Agitator Speed: 900 rpm

Run	Alloy Composition at. %			Salt Composition, mol %			Quantity Charged, kg			Run Duration, hr	CaO Conc. for Complete Reduction, mol %[a]	Reduction, % Completion
Mg-Zn-	Zn	Mg	Ca	$CaCl_2$	CaF_2	$MgCl_2$	Alloy	Salt	UO_2			
2	20	80	0	48	5	47	3.3	1.1	0.2	5	--	~90
3[b]	20	80	0	48	5	47	3.3	1.1	0.2	1	--	72
6	70	30	0	80	20	0	3.5	1.1	0.2	6	--	<40
7	70	30	0	48	5	47	3.5	1.1	0.2	5	--	89
4[b]	17	79	4	80	20	0	3.4	1.1	0.2	1	13[c]	99+
9	17	79	4	80	20	0	3.4	1.1	0.2	2	13	99+
5[b]	64	29	7	80	20	0	3.6	1.1	0.2	5	13	99+
8	64	29	7	80	20	0	3.4	1.1	0.2	5	13	99+
10	64	29	7	80	20	0	9.1	1.0	0.2	4.5	32[d]	~60
12	16	75	9	80	20	0	3.9	1.0	0.2	4.5	32	99+
11	64	29	7	100	0	0	3.6	1.0	0.2	5	13	99+
13	64	29	7	97	3	0	3.6	1.0	0.2	5	13	99+

[a] Solubility of CaO in 80 mol % $CaCl_2$-20 mol % CaF_2 at 800°C is about 15 mol %.

[b] Previously reported in ANL-7767.

[c] About 8 wt %.

[d] About 20 wt %.

$CaCl_2$-17 mol % CaF_2. It has been concluded that Zn-Mg-Ca/$CaCl_2$-CaF_2 is a practical reduction system for the head-end process.

Two runs (Mg-Zn-10 and -12) were performed to determine the practical limit of CaO loading in the salt (i.e., the maximum loading at which good separation of the salt phase from the metal phase is attained and the reduction rate of UO_2 pellets is adequate). The advantage of a high CaO loading would be to decrease the volume of waste salt that must be stored. In these runs, the quantity of UO_2 to be reduced was increased to the equivalent of a final salt composition of 32 mol % CaO-54 mol % $CaCl_2$-14 mol % CaF_2. Only the low-zinc system (run Mg-Zn-12) produced a good reduction. With the low-zinc system, the metal alloy floats on the salt and the oxide fuel and salt are mixed efficiently by the agitator. With the high-zinc system, the salt floats on the metal, and as the level of insoluble CaO in the salt builds up, the agitation (applied by a mixer in the metal phase) apparently is insufficient for adequate UO_2-salt contact. Reduction in these systems is believed to be a salt-phase reaction requiring that both the oxide fuel and the calcium be dissolved in the molten salt.

A higher CaO loading will be attempted with the low-zinc system, but no further work is planned for high CaO loadings with the zinc-rich system. Consideration will be given to possible techniques (e.g., filtration and evaporation) for concentrating the CaO waste and recycling the salt.

It is desirable that reduction product ingots fed to the HNO_3 dissolution step be free of contamination by small amounts of reduction salt since chloride and fluoride ions from this salt would corrode aqueous processing equipment. Residual $CaCl_2$ would be evaporated during the proposed vacuum evaporation to concentrate the plutonium product (Fig. I-1 and I-2), but CaF_2 is not volatile. Salt entrainment normally is very low and can be virtually eliminated by transferring product solutions over Fiberfrax, which absorbs salt readily but is not wet by metal solution.[4] As an additional precaution, it might be desirable to lower the CaF_2 content of the salt.

Two runs (Mg-Zn-11 and -13) were performed with 0 and 2.8 mol % CaF_2 in the $CaCl_2$ salt to determine the minimum concentration to CaF_2 that is associated with good separation of the salt phase from the metal phase at the end of a reduction. In each case good reductions were obtained, but in both runs the salt and metal phases did not separate well. Incremental CaF_2 additions were made to the product phases of run Mg-Zn-13. Separation improved with each addition and was good at the equivalent of 10 mol % CaF_2 in the original salt.

The only disadvantage of 90 mol % $CaCl_2$-10 mol % CaF_2 in comparison with 80 mol % $CaCl_2$-20 mol % CaF_2 is its slightly higher melting range (liquidus temperature of ∿710°C rather than ∿650°C). At 800°C, the CaO solubility in the salt having the lower CaF_2 concentration is 17 mol % as compared with 15 mol % in the salt containing 20 mol % CaF_2.

Because of the relatively high uranium solubility in 70 at. % Zn-30 at. % Mg (4 at. % or 16 wt % at 800°C),[5] this alloy is proposed for fuel reduction when dissolution of the reduced uranium in the product solution is desired. Since this reduction alloy is to contain calcium also, the effect on uranium solubility of calcium concentration in the alloy was measured. As illustrated in Table I-2, increasing the calcium concentration from 0 to 11.5 wt % suppresses the uranium solubility significantly. For a process application where dissolution of uranium is desired, it will probably be expedient to oxidize the excess calcium at the conclusion of a reduction by adding $MgCl_2$ or $ZnCl_2$ to the salt phase before agitation is stopped.

B. Process Demonstration Experiments (T. R. Johnson, W. A. Murphy, R. W. Clark)

The experimental apparatus for the demonstration of the zinc-decladding process with 100 g of irradiated fuel has been assembled and tested outside the shielded cell. Installation and testing of the equipment in the shielded facility have been started. In an experiment, an intact fuel pin will be immersed in liquid zinc to dissolve the stainless steel cladding. The oxide pellets will be collected in a tantalum basket and removed from the zinc-steel solution. Then the oxide will be reduced to metal with Zn-Mg-Ca alloy. Not only will the general processing concept be demonstrated, but also the behavior of the major classes of fission products will be studied.

Two fuel elements that were irradiated in EBR-II to a maximum burnup of 3.6 at. % at a maximum peak linear power of 13.8 kW/ft have been obtained for these experiments. The fuel is UO_2-20 mol % PuO_2 and is clad with 0.252-in. OD, 15-mil thick, 316L stainless steel tubing. The fuel was removed from EBR-II in August 1968. Information from the non-destructive testing of these particular fuel elements and from the comprehensive destructive testing of companion fuel elements from the same irradiation capsule is being obtained from Los Alamos.

C. Melt Decladding (I. O. Winsch, T. R. Johnson, T. F. Cannon, J. J. Stockbar)

Experiments have continued on separation of fuel oxide from stainless steel cladding by melting the cladding away from the fuel. The feasibility of the procedure depends upon the oxide surface being sufficiently exposed as a result of physical separation of the stainless steel so that the oxide can be completely separated in the following step (either acid dissolution or voloxidation). Exposure of the surface of the oxide pellets might be achieved by allowing the molten steel to drain away from the pellets, by pouring off the stainless steel, or by coalescing the steel as a discrete phase.

1. Melt Decladding in an Inclined Crucible

In the preceding report (ANL-7767, pp. 16-17), results were presented for runs in which bundles of twenty simulated fuel elements supported on the wall of a crucible at a 10° incline were heated so that the molten steel would flow away from the pellets. The major portion

TABLE I-2. Solubility of Uranium in Zn-Mg-Ca at 800°C

Concentration, wt %			
Zn	Mg	Ca[a]	U[b]
73.9	11.9	0	14.2
72.1	12.9	2.4	12.6
73.8	13.2	4.4	8.8
74.0	13.8	6.5	5.7
71.7	15.2	11.5	1.6
74.5	12.6[c]	9.4[c]	3.5[c]

[a] Added to original alloy as 46 wt % Ca, 36 wt % Zn, 18 wt % Mg.

[b] Filtered samples; excess uranium was present.

[c] Final addition was pure zinc.

of the steel coalesced but failed to separate from the pile of pellets. A portion of the surface of many of the pellets was wetted with steel, but all of the UO_2 was available for oxidation or for dissolution with acid.

Three additional inclined-crucible runs were made. In the first run (SSMD-7), the inclination was increased to 20° in an attempt to improve the separation of steel and oxide pellets. A bundle of 20 UO_2-containing stainless steel tubes was maintained at about 1600°C for 1 hr in an argon atmosphere at 630 mm of Hg. About 75% of the steel flowed to the bottom of the crucible, but many pellets accompanied the steel (Fig. I-3).

In similar melt decladding experiments performed at ORNL,[6] less wetting of the pellets by molten steel had been observed. Two differences between the ORNL experiments and the present tests are (1) ORNL used an Ar-4 mol % H_2 atmosphere rather than an argon atmosphere and (2) ORNL used denser pellets (>93% of theoretical density rather than 87% theoretical density).

Two runs were made to investigate why the degree of wetting differed in the two investigations. In one run (SSMD-8), a bundle of simulated fuel elements identical to those used in the preceding runs was supported on a 15° incline, heated, and maintained at 1600°C for 1.5 hr in an Ar-4 mol % H_2 atmosphere (instead of argon). The results (Fig. I-4) were not significantly different from results of other runs at ANL except that more pellets tumbled from their original position than when a 10° slope was used.

The pellets for run SSMD-17 were obtained from ORNL from the batch that they had used in their tests. The pellets (1/4-in. dia by 9/16-in. long) were assembled into ten simulated fuel elements, each containing three pellets. The bundle, supported on the wall of an alundum crucible at a 10° incline, was heated in Ar-4 mol % H_2 for 0.5 hr at 1600°C. The results (pictured in Fig. I-5) were similar to the ORNL results. About 80% of the steel flowed away from the pellets, little wetting occurred, and most of the pellets were loose. Pellet properties clearly influence the degree of wetting by molten stainless steel, but the effects on wetting of PuO_2 concentration, fission products, sodium, and irradiation are all unknown. Pending the results of conceptual design studies, no further experiments on inclined-plane melt decladding are planned.

2. Melt Decladding by Pouring Technique

Two experiments (SSMD-18 and -19) were performed in which stainless steel and UO_2 pellets (∿600 g) and fines (∿50 g) were heated in a magnesia crucible (2 1/2-in. dia, 8 in. long) to 1548°C. After the steel melted, the crucible was tilted 15° beyond horizontal to pour the steel. About 85% of the steel poured out. In run SSMD-18, the poured steel was analyzed and found to contain only 0.04% of the uranium. About 95% of the UO_2 in the crucible was loose; the balance was bonded to the steel heel. In run SSMD-19, about 6% of the pellets poured with the steel, 88% of the UO_2 (including the fines) was loose in the crucible, and about 6% was bonded to the steel heel. No additional pouring experiments are planned until a study of a conceptual design of a melt-decladding process is completed.

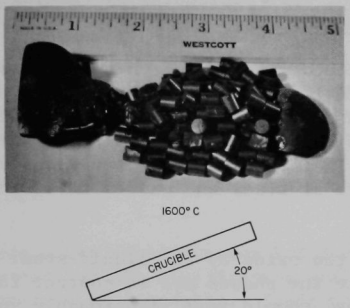

Fig. I-3. Contents of Crucible after Run SSMD-7. ANL Neg. No. 308-2424.

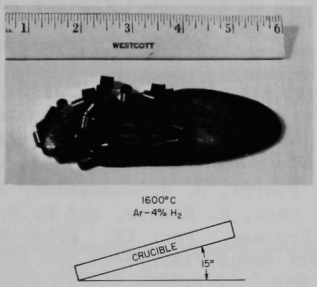

Fig. I-4. Contents of Crucible after Run SSMD-8. ANL Neg. No. 308-2425.

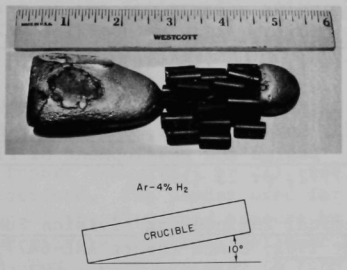

Fig. I-5. Contents of Crucible after Run SSMD-17. ANL Neg. No. 308-2471.

3. Procedure for Melt Decladding by Passing a Subassembly through a Heated Zone

In one conceptual melt-decladding process, a vertically suspended reactor subassembly is lowered into a heated zone to melt the stainless steel cladding and to release the oxide fuel pellets. Drops of molten steel and the fuel fall through a cold zone and onto a cold surface where the metal solidifies. After the larger pieces of steel are separated by screening, the mixture of steel and oxide is fed to an acid dissolver or voloxidizer.

Wetting of the oxide by the liquid steel should be minimized by this procedure because the phases are in contact for an extremely short time. The molten steel should form into roughly spherical pieces upon freezing because the surface tension of liquid steel is about 1000 dynes/cm. The spherical pieces of steel should be easier to handle than the pieces produced by shearing (in the shear-leach process), and oxide mixed with the steel particles should be dissolved rapidly and efficiently.

The experimental apparatus available is being modified for the investigation of this processing concept.

REFERENCES

1. I. O. Winsch, R. D. Pierce, D. E. Grosvenor, L. Burris, Jr., T. F. Cannon, P. J. Mack, K. Nishio, and K. R. Tobias, The EBR-II Skull Reclamation Process. Part IV. Pilot-Plant Development, USAEC report ANL-7614 (Sept. 1969).

2. J. B. Knighton and R. K. Steunenberg, Preparation of Metals by Magnesium-Zinc Reduction. Part III. Reduction of Plutonium Dioxide, USAEC Report ANL-7059, p. 10 (1965) and Trans. ANS 6, 166-167 (1963).

3. J. B. Knighton and R. K. Steunenberg, Preparation of Metals by Magnesium-Zinc Reduction. Part I. Reduction of Uranium Oxides, USAEC report ANL-7057, p. 8 (1965).

4. G. J. Bernstein, D. E. Grosvenor, J. F. Lenc, W. E. Miller, I. O. Winsch, J. Wolkoff, and R. C.Paul, The EBR-II Skull Reclamation Process. Part V. Design and Development of Plant-Scale Equipment, USAEC report ANL-7772, p. 23 (1971).

5. A. E. Martin, Chemical Engineering Division Summary Report, October, November, December 1961, USAEC report ANL-6477, p. 93 (1962).

6. D. E. Ferguson et al., Chemical Technology Division Annual Progress Report for Period Ending May 31, 1970, USAEC report ORNL-4572, pp. 53-54 (Oct. 1970).

II. CONTINUOUS CONVERSION OF U/Pu NITRATES TO OXIDES
(N. M. Levitz, D. E. Grosvenor, S. Vogler, F. G. Teats)

Conversion of uranyl nitrate hexahydrate (UNH) and plutonium nitrate solutions to powdered oxides suitable for the fabrication of fuel shapes (pellets) is a necessary and important step in the nuclear fuel cycle. Incentives for developing a new high-capacity, continuous process are the increased quantities of plutonium needed for LMFBR and plutonium-recycle fuel systems and the growing concern over shipping plutonium as nitrate solution.

A conversion process under investigation based on fluidized-bed technology developed in earlier ANL fluidization work[1] shows a high potential for meeting process requirements. Basic process steps include fluidized-bed denitration of uranyl nitrate-plutonium nitrate solutions to UO_3-PuO_2 powder, followed by fluidized-bed reduction of the UO_3-PuO_2 with hydrogen to UO_2-PuO_2 powder. The process appears to be applicable over the entire concentration range of uranium-plutonium nitrate solutions and to plutonium nitrate alone. An integrated laboratory and pilot engineering program is in progress.

In laboratory work which simulated the process, powders for preliminary evaluation and characterization containing ~20% PuO_2 were prepared by drop denitration of mixed uranium-plutonium nitrate solutions onto a heated surface, followed by hydrogen reduction (in boats). Temperatures for these two steps were approximately 300 and 550°C. Pellets were formed from this powder.

Examination of powder and pellets (see earlier reports in this series, ANL-7735, -7755, and -7767) showed that good homogeneity of the plutonium oxide in the uranium oxide matrix had been achieved. Results of recent examinations of pellet samples, given below, provide additional insight into the microstructure of material made by this process.

Successful shakedown of the denitration pilot plant by performing a series of runs with uranyl nitrate solution was reported recently (ANL-7755). Preparation of the pilot-plant for work with U/Pu materials is near completion.

A. Laboratory Program

In last quarter's report (ANL-7767, p. 21), the preparation of UO_2-20% PuO_2 pellets was described. The powder used for these pellets was obtained in a simulation of the fluid-bed process by drop denitration of uranyl nitrate-plutonium nitrate solution, followed by reduction of the denitration product, UO_3-PuO_2, with hydrogen to form UO_2-PuO_2 powder. Pellets formed from this powder had densities of 83 to 89% of theoretical. Chemical and physical analyses of pellet samples indicated that the process yields single-phase material. Results of further examination of UO_2-20% PuO_2 pellet samples to establish their homogeneity are given. Experimentally determined cosolubilities for the uranyl nitrate-plutonium nitrate-nitric acid system are also presented.

1. Electron Microprobe Examination of UO_2-PuO_2 Pellets

The purpose of the electron microprobe examination of the pellets was to determine the homogeneity of uranium and plutonium distribution in the pellet. In electron microprobe examination, a suitably mounted and polished sample is bombarded by the electron beam, and X-rays characteristic of the uranium (Mα) and the plutonium (Mβ) are emitted. The emitted X-rays are focused and counted by proportional counters. From the counting rates, the uranium-to-plutonium counting ratio is calculated. The constancy of this ratio is a meaure of pellet homogeneity. Since the intensities of the characteristic uranium and plutonium X-rays are dissimilar, the absolute actinide content cannot be determined directly from the counting rates.

Counting rates for a pellet sample were obtained with a 0.5-μm dia beam of the electron microprobe by two procedures: fixed counting at randomly selected spots and scanning of 8 by 10 μm areas and 80 by 100 μm areas, as reported in ANL-7767, p. 23. Initial measurements of selected spots with the 0.5-μm-dia beam showed uniform distribution of plutonium but considerable scatter in the counting ratio, e.g., a relative standard deviation of 20% for a series of 20 measurements of spots. Similar results were obtained in the initial measurements with the scanning method. Current work, using somewhat refined techniques, corroborated that homogeneity was good, and also gave data with improved statistics (a relative standard deviation of 8-12%).

To further check the homogeneity of a pellet, complete scans with a 0.5-μm-dia beam were made across a diameter of the pellet. In one such scan, an 80 by 100 μm area was chosen that yielded 65 counting intervals. Every tenth interval was duplicated to check instrument performance. A standard UO_2-PuO_2 pellet was scanned in a similar manner. The uranium-to-plutonium ratio was calculated for each measurement, normalized to the standard, and the average value for the series of measurements was similarly calculated. The average U/Pu ratio was determined to be 4.00 with a standard deviation of 7.8%.

Each of the individual ratios was plotted as a function of its position along the pellet diameter (see Fig. II-1). The results seem to trace a sinusoidal curve, with the first 25% of the curve showing a greater variation than the remainder of the curve. The first portion of the scan included a severe crack in the pellet, which may account for the greater scatter.

Examination of individual uranium and plutonium X-ray counting rates showed that generally both of these counting rates increased or decreased in unison, indicating that there was no appreciable localized enrichment of one of the constituents (or, conversely, no segregation of the plutonium).

In another test, a continuous scan with a 15-μm-dia electron beam was made with lithium fluoride and ammonium dihydrogen phosphate (ADP)

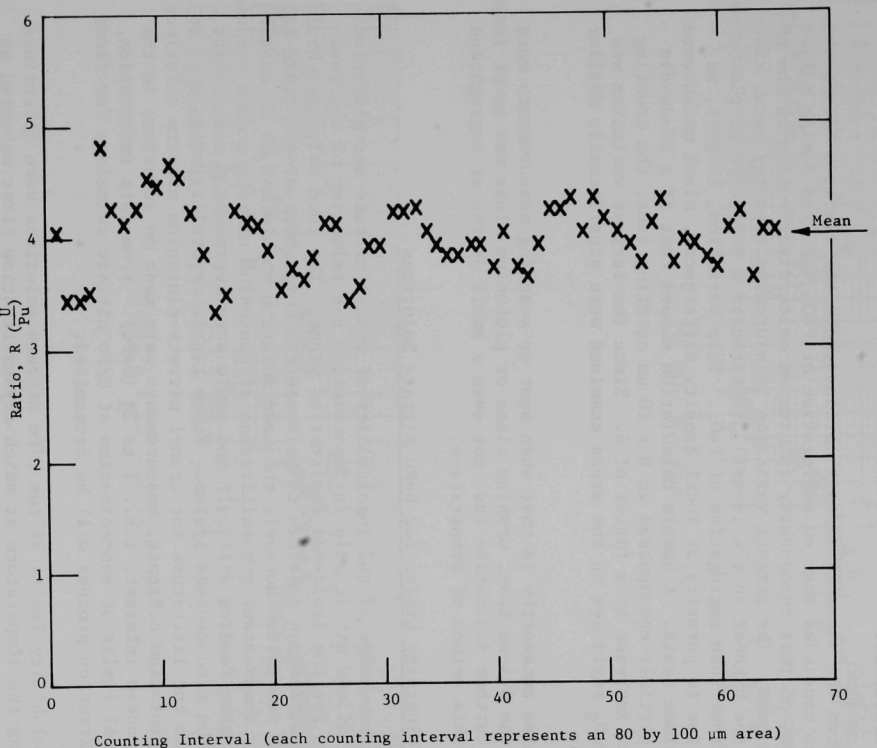

Fig. II-1. Scan of a Diameter of a 0.25-in.-dia UO_2-PuO_2 Pellet with an Electron Microprobe (Data obtained with a 0.5-μm dia beam over 80 by 100-μm areas)

crystals across the 0.25-in.-dia pellet and the uranium and plutonium counting rates were continuously recorded. In this scan (Fig. II-2), five divisions of the chart represent 1.5% of the diameter of the pellet. The scan shows that the uranium and plutonium counting rates usually moved in the same direction; this is indicative of a change in density rather than a change of concentration. A change in concentration would be indicated by the counting rate for one of the actinides increasing sharply while the other decreased.

From the accumulated data obtained with the electron microprobe, it has been concluded that no segregation of PuO_2 occurred during pellet preparation and that homogeneity (plutonium oxide distribution in the UO_2 matrix) is good. The largest variation in plutonium counting rate, about 30% (from the highest to the lowest), represented a variation of plutonium content rather than segregation of PuO_2. This variation, in part, may have been due to porosity or local density differences, since measurement is on a volume basis. A sample calculation showed that if a 50-μm-dia plutonium particle encompassed an 8 x 10 μm counting area, the counting rate should increase by a factor of 4. Since the largest variation was 30%, any PuO_2 particles in the areas examined were significantly smaller than 50 μm.

Also noteworthy is that when spot or scanning measurements were made with the 0.5-μm beam, uranium alone or plutonium alone was never found. This is a further indication that not even a small degree of segregation occurs in this method of preparation.

2. Solubility Limits for U-Pu Nitrate Solutions

A knowledge of the cosolubility of uranyl nitrate and plutonium nitrate in dilute nitric acid is important to the selection of the feed composition for the fluid-bed denitration plant. The feed solution should be as concentrated as possible to increase the throughput of the fluid-bed denitration reactors. However, the feed solution should not be so concentrated that inadvertent crystallization of plutonium nitrate occurs because this could make feeding difficult and could even represent a criticality hazard in the feed storage system. Since little crystallizlation data is available in the literature for uranyl nitrate-plutonium nitrate solutions with high plutonium contents, measurements were made on solutions in the range of process interest, i.e., 1 to 2M (U+Pu). From this information, the practical limits of concentration of U/Pu nitrate solutions for feeds in the denitration process will be determined.

Solubility limits of ten U/Pu nitrate solutions were determined by measuring the temperature at which crystallization first occurred as the solution was cooled slowly (see ANL-7767, p. 24). Ten test solutions were prepared from stock solutions of uranyl nitrate (2.52M), plutonium nitrate (1.5M), and concentrated nitric acid (16M). Approximately 30% of the plutonium was present as the hexavalent plutonyl ion.

The crystallization point was determined two or three times for each solution. For solutions with a crystallization temperature greater than 10°C, the agreement for repeated measurements was always within one degree. For crystallization temperatures below 10°C, agreement was within

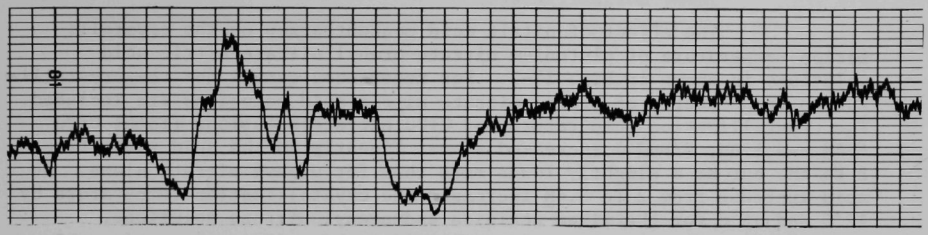

Pu (Mβ) 800 cps (LiF Crystal)

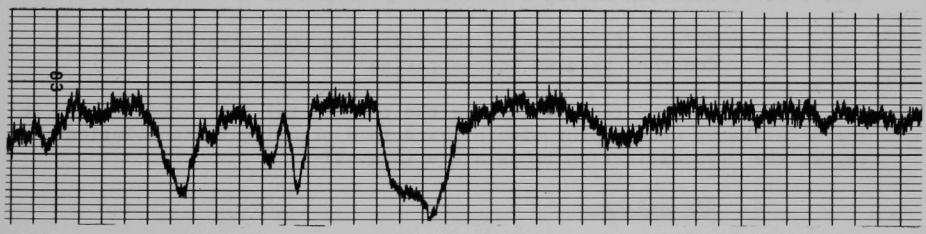

U(Mα) 4 x 10^3 cps (ADP Crystal)

Fig. II-2. Electron Microprobe Scan of a 0.25-in.-dia UO_2-20% PuO_2 Pellet (5 chart divisions = 1.5% of pellet diameter)

$\sim$1.5°C. The compositions and crystallization points of test solutions are summarized in Table II-1. Effects of individual variables are shown in Fig. II-3 to -5 and are discussed below.

a. Effect of Acidity on Crystallization Temperature

The effect of nitric acid concentration on the crystallization temperature of plutonium nitrate-uranyl nitrate-nitric acid solutions is shown in Fig. II-3. For reference, curves for the crystallization temperatures of uranyl nitrate-nitric acid solutions are included. The crystallization temperature for U+Pu nitrate solutions (total U+Pu 1.4M and 1.6M; U/Pu$\simeq$4) increased almost linearly in the acid range from 2 to 4M, but at a slightly lower rate than for uranyl nitrate alone. An acid increase from 2 to 3.4M increased the crystallization temperature by 12°C and 16°C for the mixed actinide and uranyl nitrate solutions, respectively. Beyond this point, the effect of acid concentration on crystallization temperature diminished. An acid concentration increase from 3.4 to 4.8M changed the crystallization temperatures of these solutions by only 5.6°C and 7.6°C.

b. Effect of Replacement of Uranium with Plutonium

As the fraction of plutonium in a U/Pu solution, $\frac{Pu}{U+Pu}$, was increased to 0.5 (for fixed nitric acid and fixed total heavy metal contents), the crystallization temperature decreased. For a total heavy metal content of 1.4M and with 3.4M nitric acid, crystallization temperature decreased from $\sim$13°C for a solution containing uranium only to $\sim$1.5°C for a solution having a plutonium fraction of 0.5 (see Fig. II-4).

c. Effect of Increasing the Plutonium Concentration at a Constant Uranium Concentration

As expected, increasing the total metal ion concentration in the solution by adding plutonium nitrate to a uranyl nitrate solution raises the crystallization temperature (Fig. II-5).

d. Discussion

The crystallization data reported above represent some of the points on the phase diagram of the uranyl nitrate-plutonium nitrate-nitric acid system and may be evaluated by the techniques of the phase rule. At a crystallization point, the system consists of two phases, a liquid and a solid; according to the phase rule, four degrees of freedom exist. Some of these may be fixed. In the example presented in Fig. II-4, the pressure is atmospheric, the acid concentration is 3.4M, and the total metal concentration is 1.4M. Under these conditions, the system becomes univariant and as the plutonium content changes, there is a corresponding change of the crystallization temperature. If the precipitate is assumed to be uranyl nitrate hexahydrate (UNH), Fig. II-4 shows the solubility line for a range of plutonium concentrations in equilibrium with solid UNH. Because the location of the invariant point is uncertain, the curve drawn in Fig. II-4 is tentative.

TABLE II-1. Crystallization Temperatures in the Uranyl Nitrate-Plutonium Nitrate-Nitric Acid System

Solution Composition, M				Crystallization Temp,
U	Pu	HNO_3	U/Pu	°C
1.6	0.2	2.0	8.0	13.2
1.6	0.3	2.0	5.3	15.9
1.6	0.4	2.0	4.0	18.0
1.4	0	3.4	-	12.6[a]
1.28	0.34	2.0	3.8	3.2
1.28	0.34	3.4	3.8	15.3
1.28	0.34	4.8	3.8	20.8
1.12	0.28	3.4	4.0	10.2
1.12	0.28	4.8	4.0	17.6
0.98	0.42	3.4	2.3	5.3
0.70	0.70	3.4	1.0	1.5

[a]Extrapolated from literature data on UNH solubility.

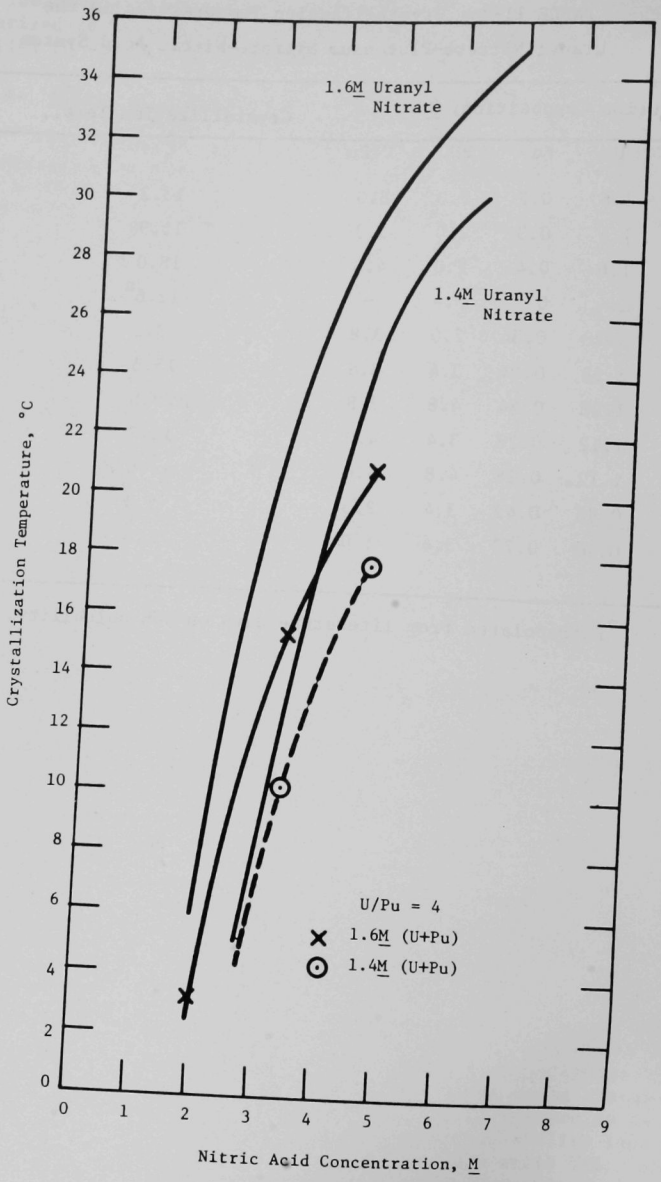

Fig. II-3. Effect of Nitric Acid Concentration on the Crystallization Temperature of Plutonium Nitrate-Uranium Nitrate-Nitric Acid Solutions

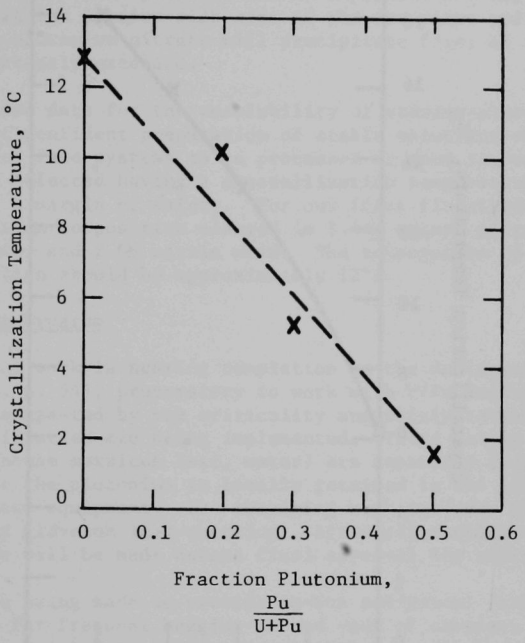

Fig. II-4. Effect of Increasing Plutonium Content upon the Crystallization Temperatures for Uranium-Plutonium Solutions

Total Heavy Metal Content: 1.4M
HNO_3 Content: 3.4M

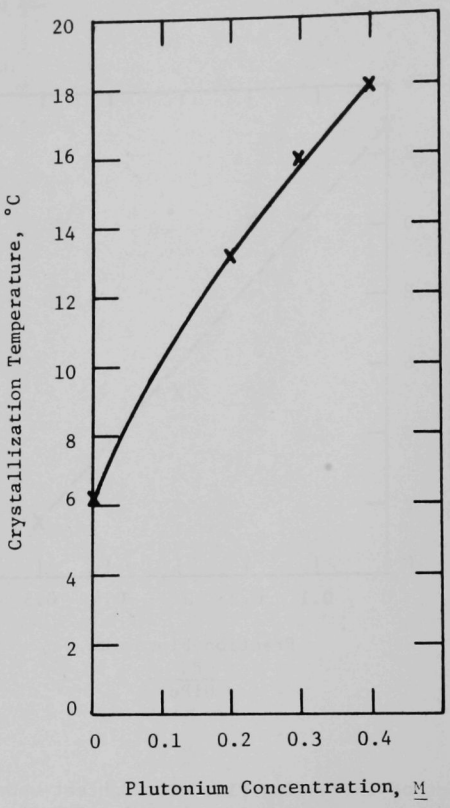

Fig. II-5. Crystallization Temperatures of Uranyl Nitrate-Plutonium Nitrate-Nitric Acid Solutions. Effect of Plutonium Conc. at 1.6M Uranyl Nitrate-2M Nitric Acid

A similar curve exists for plutonium-rich solutions; this region has not yet been examined. An effort will be made to examine this region, since such data will help locate the invariant point (where both solid UNH and solid plutonium nitrate are in equilibrium with liquid). This datum will be useful in future work.

From these data, it appears that uranyl nitrate-20% plutonium nitrate (the basic feed solution for our process work) is on the uranium-rich side of the invariant point. This is important for criticality safety because at the uranium-rich side of the invariant point, uranyl nitrate and not plutonium nitrate will precipitate first if the solubility limit is inadvertently exceeded.

These data for the cosolubility of uranium-plutonium nitrate solutions permit confident preparation of stable solutions suitable for process use. For feed systems to be processed at room temperature, a solution can be selected having a crystallization temperature of 15°C or less to provide a margin of safety. For our first fluidized-bed experiments, the solution composition planned is 1.44M uranyl nitrate, 0.36M plutonium nitrate, and 2.0M nitric acid. The temperature of crystallization for such a solution should be approximately 13°C.

B. Engineering Program

Installation work is nearing completion on the denitration pilot plant (ANL-7735, p. 54), preparatory to work with U/Pu materials. Further design changes suggested by the criticality and safety reviews of the pilot-plant auxiliaries are being implemented. These mainly concern assurance that house services (air, water) are separated from the installation, and that the plutonium is totally retained in the glovebox that houses the process equipment. The remaining work includes glovebox window installation and glovebox leak-checking. After all changes are completed, a further review will be made before final approval for startup is given.

Efforts are being made to provide in-box analytical facilities to reduce the need for frequent bagging-in and -out of samples. For example, a Ge-Li detector coupled to a 256-channel analyzer will be tested at a glove-port position for possible direct plutonium analysis of solutions by gamma counting. It is also planned to install titration equipment for acid and uranium analysis in the glovebox. A small enclosure within the glovebox (essentially a box within a box) will be used for handling powders; this should minimize the spread of powder and simplify housekeeping.

Reference

1. A. A. Jonke, E. J. Petkus, J. W. Loeding, and S. Lawroski, Nucl. Sci. Eng., 2, 303 (1957).

III. IN-LINE ANALYSIS IN FUEL FABRICATION
(J. G. Schnizlein, T. Gerding, M. J. Steindler)

The development of rapid, precise, and accurate in-line nondestructive methods for the analysis of critical properties of reactor fuel will lower fuel fabrication costs for the large number of fuel pellets that will be processed in the LMFBR program. For this evaluation of analytical methods, the starting criteria selected are the specifications of pre-irradiation fuel properties (and the associated precisions) for the Fast Flux Test Facility (FFTF) project. The fuel properties, specifications, precisions, and acceptable methods of measurement for the FFTF were discussed in an earlier quarterly report (ANL-7735, pp. 59-66). As additional information on the relationship between fuel properties and fuel performance is obtained from irradiation experiments, more realistic and possibly less rigorous specifications for fuel properties are expected.

The fuel for the first commercial FBR is expected to be uranium-plutonium oxide. Two fuel properties have been selected for initial study because their determination is necessary in every conceivable fabrication procedure: plutonium/uranium (Pu/U) ratio and oxygen/metal ratio in uranium-plutonium oxide. A literature study indicating that oxygen/metal ratios can be determined by measurement of lattice parameters is described in ANL-7735, pp. 65, 71-80.

A. Plutonium/Uranium Ratio in Fuel

The most rigorous specification on plutonium content for FFTF fuel is for a core zone that must have an average plutonium content of 20.0 $\pm$ 0.1%. This requires a precision of $\pm$0.5% for any applicable analytical method. X-ray fluorescence (XRF) analysis is being evaluated as an in-line analytical method for determining Pu/U ratio in UO_2-PuO_2 fuel materials. XRF analysis is a sensitive, nondestructive method in which exciting radiation impinges on the sample and causes the emission of radiation that is characteristic of the elements present; by application of this method, uranium and plutonium concentrations can be determined rapidly and accurately enough to be practical at high fuel-production rates. In the experimental program to demonstrate the practicality of this analytical method, not only the material effects but also the instrumental choices and sample presentation procedures are being defined.

Initial investigations are being done with ThO_2-UO_2 as a stand-in for UO_2-PuO_2 to avoid the inconvenience of handling plutonium. This substitution is practical because of the identical relationship of the atomic numbers of each pair of elements and thus of the relevant properties (see ANL-7726, pp. 141-142). Part of the data obtained with ThO_2-UO_2 will later be verified in experiments with UO_2-PuO_2.

1. Discussion of Possible Interfering Impurities

Emission lines of impurity elements that might possibly interfere with the X-ray fluorescence analysis of UO_2-PuO_2 can be identified by consulting a tabulation of known spectra for lines between 12.5 and 14.9 keV. Portions of such a table (presented in Table III-1) show a small group of K spectra lines, a larger group of L spectra lines (which includes

TABLE III-1. X-Ray Critical-Absorption and Emission Energies in keV[a]

Atomic Number	Element	Symbol	K Series					L Series								
			K_{ab}	$K_{\beta 2}$	$K_{\beta 1}$	$K_{\alpha 1}$	$K_{\alpha 2}$	L_{Iab}	L_{IIab}	L_{IIIab}	$L_{\gamma 1}$	$L_{\beta 2}$	$L_{\beta 1}$	$L\alpha_1$	$L_{\alpha 2}$	
RELATIVE INTENSITY				3	21	100	50				10	20	50	100	20	
34	Selenium	Se	12.652	12.651	12.495											
35	Bromine	Br	13.475	13.405	13.290											
36	Krypton	Kr	14.323	14.313	14.112	12.648	12.597	Th								
37	Rubidium	Rb	15.201			13.394	13.335	U								
38	Strontium	Sr	16.106			14.164	14.097	Pu								
39	Yttrium	Y	17.037				14.882									
77	Iridium	Ir						13.413	12.819	11.211	12.509					
78	Platinum	Pt						13.873	13.268	11.559	12.939					
79	Gold	Au						14.353	13.733	11.919	13.379					
80	Mercury	Hg						14.841	14.212	12.285	13.828					
81	Thallium	Tl						15.346	14.697	12.657	14.288					
82	Lead	Pb						15.870	15.207	13.044	14.762	12.620	12.611			
83	Bismuth	Bi						16.393	15.716	13.424		12.977	13.021	Th		
84	Polonium	Po						16.935	16.244	13.817		13.338	13.441			
85	Astatine	At						17.490	16.784	14.215		13.705	13.873	U		
86	Radon	Rn						18.058	17.337	14.618		14.077	14.316	Pu		
87	Francium	Fr						18.638	17.904	15.028		14.459	14.770			
88	Radium	Ra						19.233	18.481	15.442		14.839				
89	Actinium	Ac						19.842	19.078	15.865					12.499	
90	Thorium	Th						20.460	19.688	16.296				12.966	12.808	Th
91	Protactinium	Pa						21.102	20.311	16.731				13.291	13.120	
92	Uranium	U						21.753	20.943	17.163				13.613	13.438	U
93	Neptunium	Np						22.417	21.596	17.614				13.945	13.758	
94	Plutonium	Pu						23.097	22.262	18.066				14.279	14.082	
95	Americium	Am						23.793	22.044	18.525				14.618	14.411	Pu
96	Curium	Cm						24.503	23.640	18.990					14.743	
47	Silver	Ag	25.517	25.454												
48	Cadmium	Cd	26.712	26.641	26.093	23.172	22.982									
49	Indium	In	27.928	27.859	27.274	24.207	24.000									
50	Tin	Sn	29.190	29.106	28.483	25.270	25.042	Th								
51	Antimony	Sb	30.486		29.723	26.357	26.109									
52	Tellurium	Te	31.809			27.471	27.200	U								
53	Iodine	I	33.164			28.610	28.315									
54	Xenon	Xe	34.579			29.802	29.485	Pu								

[a]Reprinted with permission from Philips Electronic Instruments.

spectra lines of the actinide elements), and a small group of second-order K spectra (E = 1/2 of primary energy) which might possibly interfere. Each of these groups has been divided into regions of interference with the plutonium, uranium, and thorium analyses as follows:

	$L\alpha_1$ Emission Line, keV	Range for Possible Interference
Pu	14.279	13.94-14.61
U	13.613	13.34-13.94
Th	12.966	12.65-13.34

The line intensities of impurities at the expected or specified concentrations in fuel material were compared with the line intensities of plutonium, uranium, and thorium at their expected concentrations. Most of the interfering elements are rare and would not be expected in purified process materials. Their lines are of such low intensity that interference could occur only if they were present in concentrations similar to or greater than the uranium or plutonium concentrations.

The elements first considered were those which appear in the specifications of maximum impurity contents and also are potential interferences:

Cd		<20 ppm
Ag,Pb,Sn	sum with Mn, Mo	<200 ppm

Only the second-order K spectra of Cd, Ag, and Sn could interfere. The second order spectra would be about one-tenth the primary intensity--for Cd, the Kβ2 is only 3% of the Kα1; for Sn, the Kβ1 would be only 21% of the Kα1. It is doubtful that 20 to 50 ppm of any of these elements could be detected above the background, much less interfere.

Within the group of elements having L spectra in a region of possible interference, only Pb and the actinides, Pa, Np, Am, and Cm, merit any further comment. Pb Lβ2 is only included as a possible interference for Th and it would be adequately resolved for U and Pu analysis. None of the actinides Pa, Np, Am, and Cm would be present in the Pu used in fabrication of FFTF fuel at a high enough concentration to affect the plutonium analysis by 0.1%, even assuming that no resolution of the interfering actinide and the fuel component is accomplished. If these actinides are in future fast reactor fuels during fabrication or recycle, they might have to be considered as possible interferences, depending on the required precision of the analysis.

All elements having K spectra in a region of possible interference were next considered. Only strontium merits consideration. The strontium Kα lines could interfere with the analysis of plutonium. In fact, the interference was observed in work a few years ago on fluidized-bed fluorination of simulated UO_2-PuO_2-fission product oxides.[1] When strontium and plutonium were present at similar concentrations (0.01 to 1.0%), the line intensities of PuLα and SrKα were of similar magnitude.

Assuming no resolution, 1000 ppm strontium would contribute counts similar to 0.1% Pu. Therefore, in a fuel containing 20% plutonium, 1000 ppm but not 100 ppm strontium would prevent attaining a precision of ±0.1%. The FFTF specification of 250 ppm for calcium makes it extremely unlikely that the chemically similar strontium (which might be incorporated with calcium) would be present at a concentration in excess of 100 ppm.

It can be concluded that within the series of elements having K spectra in a region of possible interference, strontium is the only possible interference if present at a concentration greater than 100 ppm. For future LMFBR fuels, the concentrations of the actinide elements Pa, Np, Am, and Cm in the plutonium will have to be considered.

2. Instrumental Considerations

In the absence of other limitations, the precision of X-ray fluorescence analysis is limited by counting statistics (ANL-7735, p. 71)--that is, precision is improved at higher total counts. Any modifications that decrease the time to reach a count corresponding to the desired precision will improve the opportunity for in-line application as well as the accommodation to higher production rates. Equipment modifications are desired that will increase uranium and thorium count rates without excessively increasing the background rate.

Data presented last quarter (ANL-7755, pp. 46-47) demonstrated that 20-mil slit widths in the collimators (instead of the usual 5-mil slit widths) give adequate resolution of the uranium and thorium peaks and also increase counting rates tenfold. The counting rate for uranium was observed to increase to 7×10^3 cps. At this count rate, a counting time of 0.5 min will yield a precision of ±0.5% at the 95% confidence level. If the thorium peak and background are then counted sequentially, the total counting time for each pellet is estimated to be about 1 min.

a. Reproducibility of Sample Presentation

An aluminum sample holder of new design (ANL-7767, p. 27) was constructed that provides reproducible loading. Samples of powder or pellets are loaded in the sample holder so that the surface of the powder or pellets is even with the cup rim. With this sample holder and loading procedure, the counting rate has been increased by a factor of 1.5 and the background count (from scattered X-rays) decreased by a factor of 3. Hence, the analysis time has been decreased and the precision improved.

A series of measurements were made to establish the X-ray spectrograph counting stability, the reproducibility of sample placement relative to the primary X-ray source, and the reproducibility of sample loading. Counting stability was measured by repetitive counting of a sample of UO_2 for a fixed time. The relative standard deviation of ten measurements was 0.1%. The measurement of reproducibility of sample placement relative to the primary X-ray source was done by withdrawing and replacing the sample carrier in the instrument and counting for a fixed time. The standard deviation of ten measurements was 0.1%. The reproducibility of sample loading was tested by completely reloading the powder sample and counting for a fixed time. The standard deviation of ten measurements

was 0.16%. At the 95% confidence level, $2\sigma = 0.34$, which is within the required total uncertainty.

These results demonstrate that adequate reproducibility ($\sigma \leq 0.2\%$) can be achieved by standardizing the replacement of the sample carrier and the loading of powder samples.

b. Dead Time and Coincidence Corrections

New Norelco counting equipment, manufactured by Philips Electronic Instruments Inc., has been put into operation that includes a scintillation detector (No. 850-101) and a data control and process panel (No. 130-100-23) with pulse height analysis option. With this counting equipment and the new sample-presentation method, uranium count rates up to 1.8×10^4 cps can be measured for 20% UO_2-80% ThO_2 samples, and count rates of about 9×10^4 cps can be measured for pure materials.

Corrections for dead time and coincidence, required at count rates above 3×10^4 cps, have been calculated. In the calibration of the Norelco detector and counting equipment for efficiency at high counting rates, X-irradiation of a 1/4-in. uranium metal sample in the holder by operating the tungsten-target X-ray tube at 59 kV and 41 mA provided about 9×10^4 cps. The method for calibration of the detector and counter utilized "paired sources" counted separately and together. This provided counts in increments that varied by factors of two. The use of absorbers of about "half thickness" allowed the calibration to be performed in situ on radiation in the range of primary interest.

In two separate series of experiments, the count rate was decreased (through 8 or 12 increments) from 9×10^4 cps to about 900 cps by placing nickel or aluminum absorbers of various thicknesses between the crystal analyzer and the detector. The aluminum absorbers were manufactured by Tracerlab, and the nickel absorbers were 0.35-mil foil. Count rates were measured with the spectrometer set on the uranium Lα emission line. The nickel absorber was used in the final calibration because it has a higher ratio of photoelectric to scattering cross section; this ratio is 71 for nickel and 16.5 for aluminum. It was verified at low count rates (R) that the least-squares fit provided a slope (log R vs mg/cm^2 absorber) equal to the expected[2] absorption coefficient of the absorbers (i.e., 10.8 cm^2/g for aluminum and 90 cm^2/g for nickel) for 13.6 keV (ULα) X-radiation. From these data, a corrected count rate for each observed count rate in this calibration can be calculated, and these data can be used to calculate a correction factor relationship for the counter.

The relationship for correction of high count rates that was chosen was as follows:

$$I = M + 2.876 \times 10^{-6} M^2 + 1.47 \times 10^{-11} M^3 \qquad (1)$$

where M and I are measured and corrected count rates. In duplicate experiments, the coefficients were determined by a least-squares fit, resulting in a standard deviation of 33 cps for I (over the range of M from 900 to 90,000 cps) and relative standard deviations of 0.9 and 2.5% for the coefficients of M^2 and M^3. It is still necessary to define whether the

precision of the analysis is limited by material properties.

3. Material Effects

The fluorescence intensity of a characteristic radiation is influenced by two kinds of matrix effects--absorption and enhancement. To attain the required precision in the analysis of solid oxide as powder or pellets, absorption and enhancement must be proved to be either insignificant or predictable.

Absorption includes the effects of scattering from the surface, voids, and crystallites, as well as absorption described by the mass absorption coefficients of the elements present. Enhancement (or secondary fluorescence) occurs when the characteristic radiation from one component element has enough energy to excite the characteristic radiation of the element being measured. This occurs in uranium-plutonium oxides because PuLα excites ULα. In thorium-uranium oxides, ULα excites ThLα.

Normally, quantitative analysis by a fluorescence technique requires a set of standards covering the ranges of variables of interest, such as composition (element concentration and matrix content), density, crystallite size, and absorption coefficients. Criss and Birks[3] have formulated calculational methods whereby X-ray fluorescence intensities can be calculated from fundamental parameters. Computer calculations should greatly decrease the number of standards necessary by allowing some prediction of signal losses due to material effects.

This quarter, reproducibility of fluorescence data has been measured for powder and pellets with various urania and thoria concentrations. This work will be followed by determination of the working curve or empirical coefficients to relate signals to concentrations and account for enhancement and particle size effects. Later experimental work will be with samples having a range of plutonium contents to demonstrate whether the necessary precision can be attained despite variations in powder properties such as particle size, bulk density, and O/M ratio.

a. Uranium Content of UO_2-ThO_2 Mixed Powder

Measurements of the intensity of the Lα emission line from uranium and thorium were determined for powder mixtures of 10, 15, 20, 25, and 30 wt % UO_2 in ThO_2. The mixtures were prepared from pure ThO_2 and from UO_2 that had been reduced from NBS U_3O_8. Thorium, uranium, and oxygen contents of each of the pure oxides were verified by analysis.

Four sets of data of the intensity of the element peak compared with the intensity of the peak for pure oxide have been collected for powder mixtures and corrected for errors due to high count rates. The relative standard deviations for each concentration range were 0.28 and 0.37% for uranium and 0.78 to 2.2% for thorium. Factors that contribute to this error include instrumental and sample properties. The latter include as-yet-unresolved sampling uncertainties (which may result in variation of UO_2 content), as well as differences in particle size distribution. As more information on the influence of particle size and bulk density is acquired, some of the deviation can be assigned to appropriate factors and the data

corrected.

b. Analysis of Pellets

Four pellets have been prepared from each of the mixed powders, 10, 20, and 30% UO_2 in ThO_2, and from pure UO_2 and pure ThO_2. The pellets were sintered in 6% H_2-He atmosphere at 1750°C for 4 hr. Shrinkage occurred during sintering of the mixed-oxide pellets in proportion to their thorium content (which ranged from 90 to 70%). Direct comparisons of signal strength of the uranium emission line of the pellets and the powder samples (subsection "a" above) must await correction for the reduction in the sample area exposed to the beam.

Initial fluorescence measurements on the pellets indicated a considerable variability in the count rate for a given pellet. Microscopic examination of the pellets showed irregularities of the surface. Hand-polishing with 600-grit silicon carbide paper improved the reproducibility approximately twofold to relative standard deviations of 0.65 and 0.03% for uranium and thorium, respectively. Greater attention to the mixing of UO_2 and ThO_2 prior to pellet formation should yield the reproducibility required. The improvement in reproducibility effected by producing a flat surface on the pellets (described in section 2a above) indicates that the condition of the sample surface is important to the precision of the fluorescence.

4. Conclusion

The X-ray fluorescence method utilizing thoria-urania mixtures as a stand-in for urania-plutonia continues to show promise of achieving a relative precision of 0.5% for powders and pellets.

REFERENCES

1. Chemical Engineering Division Annual Report, 1968, USAEC Report ANL-7575, p. 48 (April 1969).

2. W. H. McMaster et al., Compilation of X-ray Cross Sections, Sec. II, Rev. 1, USAEC report UCRL-50174 (May 1969).

3. J. W. Criss and L. S. Birks, Anal. Chem. 40, 1080 (1968).

IV. ADAPTATION OF CENTRIFUGAL CONTACTORS IN LMFBR FUEL PROCESSING
(G. Bernstein, J. Lenc, N. Quattropani)

The performance characteristics of centrifugal contactors suitable for use for plutonium purification (plutonium-isolation steps) in the Purex-type solvent extraction of LMFBR fuel material are being investigated. A contactor design is being studied in which the diameter of the contactor is limited to geometrically favorable dimensions in order to minimize criticality hazards related to the high plutonium concentrations in the process streams.

Other expected advantages of centrifugal contactors are reduced radiation damage to the solvent as a result of brief residence time in the contactor and improved ease of operation (including rapid flushout at the end of a processing campaign).

A. Equipment Testing

A stainless steel contactor (ANL-7735, p. 84) has been fabricated and installed in a contactor test facility. An overall view of the assembled contactor before installation is shown in Fig. IV-1. The rotor and removable mixing paddle are shown in Fig. IV-2. The rotor has a 4-in. ID, a 12-in.-long settling zone and a 3-in.-long weir section. It was designed to operate at speeds up to 3600 rpm and to have a separating capacity* of about 10 gpm (total for both phases) at the maximum speed. Since stable rotation at high speed is required for good overall performance, dynamic stability tests were made of the rotor components during fabrication, and the finished rotor after assembly. Results showed that the rotor was well balanced. Final dynamic testing was done with the complete contactor assembly mounted in the test facility. The vibration at a rotor speed of 4000 rpm was very low, indicating that the degree of precision exercised in fabrication was sufficient to meet the rigid design specifications.

B. Procedure, Results, and Discussion

Preliminary runs to evaluate hydraulic and mechanical performance of the centrifugal contactor were carried out at rotor speeds of 2000 to 3500 rpm, using 0.03M HNO_3 as the aqueous phase and Ultrasene (refined kerosene) as the organic phase. Additional runs were done at these rotor speeds with 0.5M HNO_3 as the aqueous phase and 15% tributyl phosphate (TBP) in Ultrasene as the organic phase. The latter solution more closely resembles solutions used in Purex-type processes. Operating conditions and results are summarized in Table IV-1.

On the basis of the current results, the design goal of 10 gpm at a rotor speed of 3600 rpm was achieved. At a rotor speed of 3500 rpm, separating capacities were significantly higher with the acid-Ultrasene system (~18 gpm) than with the acid-TBP-Ultrasene system (~10 gpm). The higher separating capacity obtained with the acid-Ultrasene system is attributed to the formation of mixtures that are much easier to separate than those obtained with the acid-TBP-Ultrasene system.

*Separating capacity is arbitrarily defined as the maximum total flow throughput with no more than 1 vol % entrainment of either phase in the exit stream of the other phase.

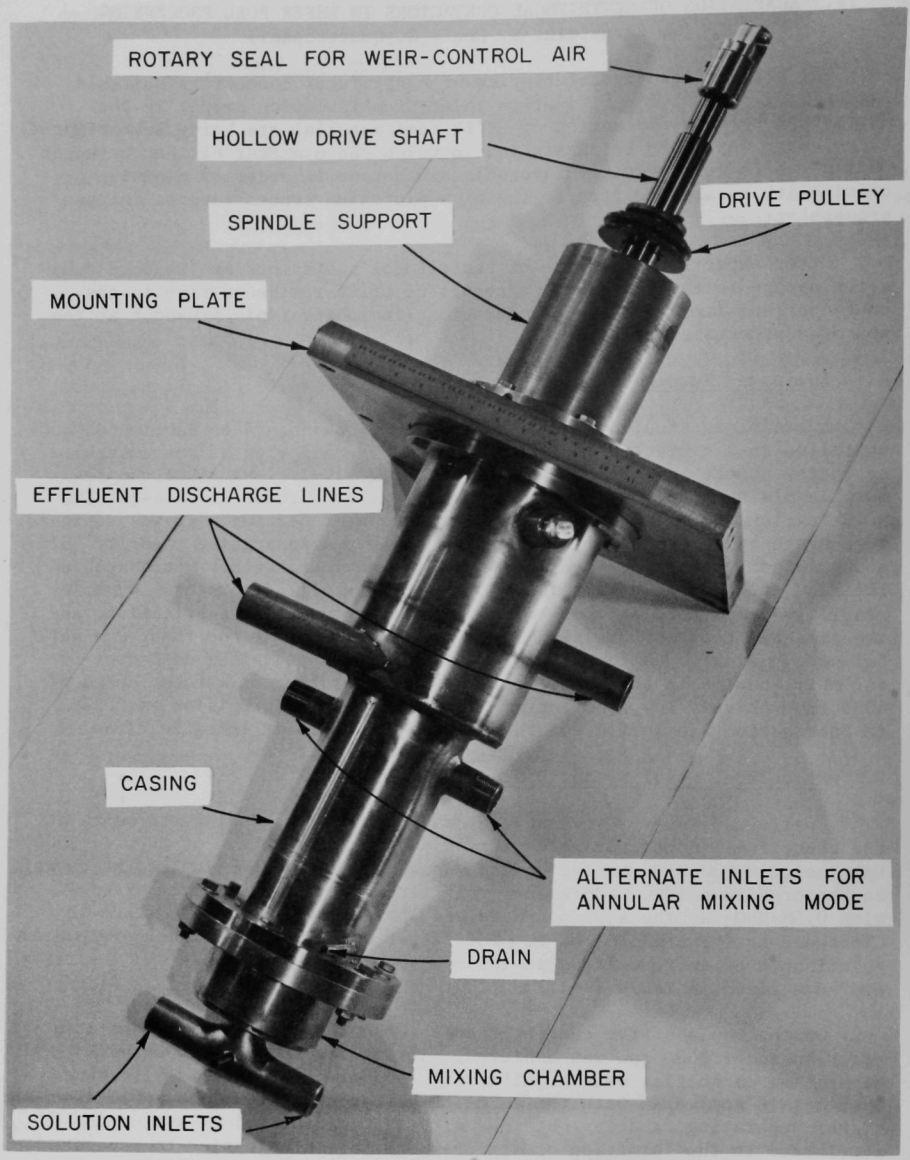

Fig. IV-1. Centrifugal Contactor Assembly.
ANL Neg. No. 308-2361A.

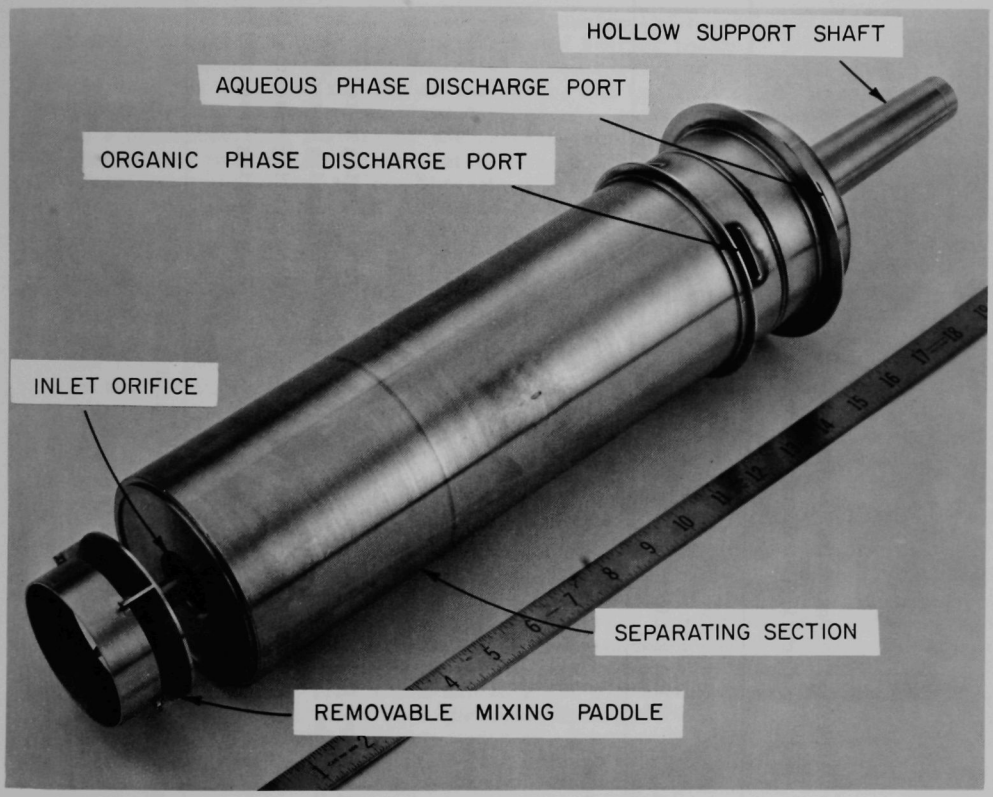

Fig. IV-2. Rotor and Removable Mixing Paddle.
ANL Neg. No. 308-2354A.

TABLE IV-1. Operating Conditions and Results,
Centrifugal Contactor Runs

Molarity of Nitric Acid Aqueous Stream	Organic Stream	Aqueous-to-Organic Flow Ratio (A/O)	Rotor Speed (rpm)	Separating Capacity (gpm)	Remarks
0.03	Ultrasene	1:1	2000	10	
		1:1	3500	18	
		1:2	2000	10	
		1:2	3500	14	a
		1:3	2000	10	
		1:3	3500	12	a
0.5	15 vol % TBP in Ultrasene	1:1	2000	4	Flow surging noted
		1:1	3500	6.2	Flow surging noted
		1:1	2000	5.6	Flow surging essentially eliminated
		1:1	3500	10	Flow surging essentially eliminated

[a]Total throughput probably limited by capacity of inlet piping.

In runs with the acid-Ultrasene system, separating capacity at high rotor speeds and low aqueous-to-organic (A/O) ratios was limited by flow restrictions rather than by separating capacity of the rotor itself. With the inlet piping restricting the organic stream flow rate to about 9 gpm, the maximum capacity was found to be 14 gpm at an A/O ratio of 1:2 and 12 gpm at an A/O ratio of 1:3. Replacement of the inlet piping system with larger pipes is planned to permit determination of the full separating capacity of the unit.

Mechanical performance was very good during these test runs, as indicated by little heatup of the shaft and bearing region. Interface control by means of the air-controlled aqueous-phase weir was also good. (By means of weirs at the top of the rotor, the two phases are directed into separate collector rings and discharged. An emulsion band, which is a characteristic feature of the aqueous-organic interface in centrifugal contactors, must be positioned between the aqueous and organic weirs to minimize contamination of one phase by the other.) Weir-control pressure ranged from about 1 to 4 psig, depending on flow rates and rotor speed.

1. Flow Surging

At the start of the tests and again later during tests with TBP, flow surging in both streams was noted. Surging is believed to contribute to a reduction in separating capacity, since variations in flow rate through the rotor can cause shifting and widening of the emulsion band at the top of the rotor, leading to excessive entrainment of one phase in the other.

Surging was attributed to excessive pumping capacity of the mixer-pump with resultant air gulping. The pumping capacity was also believed to be enhanced by the ring attached to the paddle (see Fig. IV-2). This ring was incorporated in the paddle design to improve the dynamic stability of the overhung rotor. The ring may serve to isolate some of the fluid mixture from the baffles located on the chamber wall and thus increase the extent of swirling, which contributes to pumping capacity.

Two changes in the mixing chamber baffle arrangement were made in the course of the tests to reduce the pumping and surging effect. During the tests with the acid-Ultrasene system, increasing the length of the four 1/4 in.-wide baffles from 1 1/2 in. to 2 in. significantly reduced the flow surging. During the tests with the acid-Ultrasene-TBP system, four additional baffles (3/8 in. wide and 2 in. long) were installed between the original baffles. Under these operating conditions, the capacities shown in Table IV-1 were achieved.

V. ELECTROLYTIC REDUCTION AND REOXIDATION OF PLUTONIUM IN PUREX PROCESSES

(M. Krumpelt, J. Heiberger, M. J. Steindler)

The Purex solvent extraction process[1] is being studied and evaluated for the reprocessing of spent LMFBR fuels.[2] Among the characteristics of these fuels that make reprocessing a potentially difficult task is their high plutonium content. For example, for the AI reference fuel, the plutonium concentration in the core is 19% and that in the combined core and blanket fuel is ~8%.[3] In the Purex process, a change of valence of plutonium is carried out during plutonium partitioning and isolation steps to achieve the desired level of decontamination. Tetravalent plutonium is extracted very favorably into a TBP-dodecane phase from a nitric acid solution. Trivalent plutonium, in contrast, is almost insoluble in this organic system. By changing the valence state of plutonium, it can be cycled between the organic and the aqueous phases until the plutonium is adequately separated from fission-product contaminants.

Currently, valence changes are accomplished by chemical means that have the following disadvantages: (1) they may increase the quantity of highly active wastes to be disposed of (significantly increasing the cost for waste storage), (2) they may require undesirable changes in parts of the flowsheet,* (3) they may necessitate lengthy operations external to the main process stream, and (4) they may interfere with other Purex process steps.** Also, reduction with chemical reagents requires the storage and handling of unstable reducing agents. For these reasons, direct electrolytic methods for plutonium valence adjustment are being examined for use with centrifugal contactors (which offer two requisites for an economic process: high throughput and attendant nuclear safety).

A. Review of the Problem of Valence Adjustment

The basic Purex flowsheet[1] for the plutonium purification cycle(s) includes feed adjustment, extraction, scrubbing, and stripping steps. The feed to the Purex process is a nitric acid solution containing plutonium. In the feed adjustment step, the valence of plutonium in the nitric acid solution is raised from the 3+ to the 4+ oxidation state with sodium nitrite in preparation for extraction into the organic phase and scrubbing. Later, to facilitate recovery of the plutonium from the organic phase (i.e., stripping), the plutonium valence is reduced to the 3+ oxidation state with ferrous sulfamate; the ferrous ion reduces plutonium (IV), and the sulfamate stabilizes the resulting solution by preferential reaction with any nitrous acid. Final purification, including some decontamination and iron removal, is presently achieved by ion exchange (which is a relatively low-capacity process step). The product is a plutonium nitrate solution suitable for further processing steps such as concentration, conversion to oxide, and

---

* Contamination of the plutonium product with chemical reducing agents necessitates additional process steps prior to conversion of plutonium solutions to the dioxide.

** Reductants that remain in aqueous streams after plutonium has been extracted often prevent recycle of these streams to other parts of the process; as a result, waste volumes are larger and product losses higher.

fuel fabrication. The use of sulfamate has shortcomings,[4] however, which have led to the use of uranous nitrate as a reducing agent in plants such as the British,[5] French,[6] and Eurochemic[7] installations. Ferrous nitrate with hydrazine as a stabilizer has also been proposed[8] as a substitute for ferrous sulfamate. Recently, hydroxylamine nitrate has been proposed as a reducing agent.[9]

As stated above, sodium nitrite is being used for the oxidation of Pu(III) to Pu(IV). Alternative oxidants that recently received some laboratory-scale attention[10] in a LMFBR fuel reprocessing scheme are gaseous mixtures of $NO-NO_2$. The two oxidants are chemically equivalent in the Purex process since both are converted to nitrous acid in an aqueous medium. The reaction of plutonium (III) with nitrous acid is fairly fast and autocatalytic;[11] the nitrous acid is regenerated by reaction of nitric acid with NO, a product of the oxidation:

$$Pu^{3+} + HNO_2 + H^+ \rightleftarrows Pu^{4+} + H_2O + NO$$

$$2\ NO + HNO_3 + H_2O \rightleftarrows 3\ HNO_2$$

Excess nitrous acid in the solution, which could interfere with the plutonium stripping step, can be eliminated by purging with air.

Development work on electrolytic reduction is under way at Karlsruhe[12,13] but is focussed on the partitioning cycle. The work at Argonne is primarily directed toward plutonium isolation in the Purex process, namely, the second and third extraction cycles. Electrolytic reduction is more difficult in these cycles than in the partitioning step because the catalytic role of uranium cannot be relied on (see Section B below). However, the potential advantages of electrolysis are greatest in the third cycle; if chemical reductants are absent, the product of the third cycle can be directly denitrated to PuO_2.

The nitrous acid method described above for oxidizing Pu(III) generates no solid waste but creates an NO off-gas stream. Although the increased NO volume could be reoxidized and recycled in LMFBR fuel reprocessing, the NO and hence the recycling equipment and operation could be eliminated by electrolytic oxidation of Pu(III). In addition, because excess nitrous acid is added in the conventional oxidation step, an excess of reductant may be needed in the subsequent step.

Electrolytic processes are amenable to more precise control and do not require excess reagents. However, no work has been reported on electrolytic oxidation of plutonium.

B. Review of Plutonium and Uranium Electrolysis

Cohen[14] made the first systematic study of reducing different plutonium valence states electrolytically. He used a three-compartment cell for the anode, cathode, and reference electrode, respectively. The cathode and anode were platinum wires. The electrolyte was 1M $HClO_4$. Current-voltage curves were measured potentiostatically at 25°C for various plutonium ions. Cohen's results are reproduced in Fig. V-1, because they illustrate the electrolysis. The standard equilibrium potential of the $Pu^{4+} + e^- \rightleftarrows Pu^{3+}$

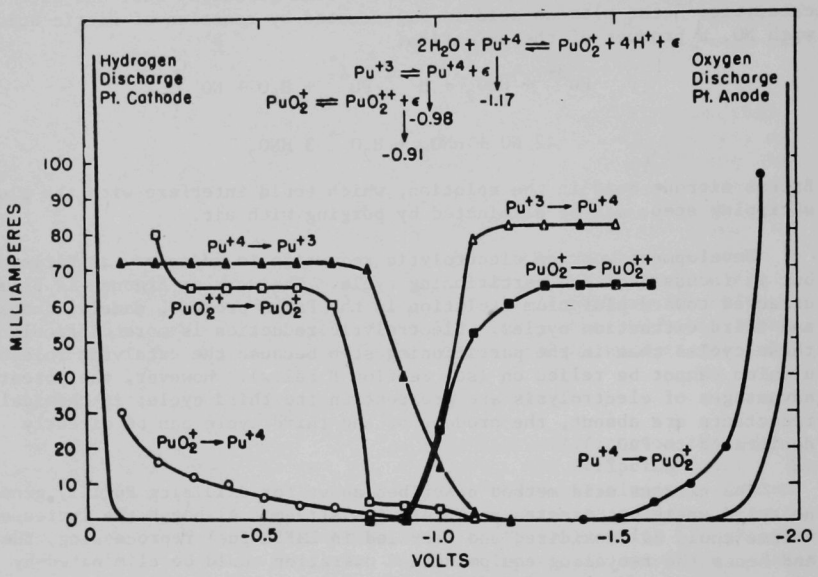

Fig. V-1. Current-Voltage Curves for Plutonium Ions in 1M $HClO_4$. Reprinted with permission of D. Cohen, J. Inorg. Nucl. Chem. 18, 209 (1961), Pergamon Press.

reaction in 1M $HClO_4$ is +0.982 V.* A slightly different equilibrium potential of +0.932 V has been measured in 1M HNO_3 for the Pu(III) - Pu(IV) couple.[15] The difference is attributed to the formation of complex ions by Pu(IV).

Figure V-1 shows that the reduction of Pu(IV) and the oxidation of Pu(III) proceed well near the equilibrium potential and that limiting currents are reached in both directions at only slightly different potentials. These low overpotentials suggest a reversible reaction, which was proved to be the case in a later chronopotentiometric study.[16] At the counter electrode, oxygen is formed during the reduction of Pu(IV) and hydrogen is formed when oxidizing Pu(III). The electrode reaction on an oxygen electrode in acidic medium is

$$O_2 + 4\ H^+ + 4e^- \rightleftarrows 2\ H_2O \qquad E^\circ = +1.229$$

In Cohen's work, a potential of 1.8-1.9 V was necessary to drive the reaction toward oxygen evolution. An overvoltage of 0.6 V is common for oxygen-discharge electrodes. Because of this high overvoltage on the anode, Cohen had to apply a potential greater than 1 V between anode and cathode to reach the limiting current density. The standard potentials in HNO_3 indicate a difference of only $\sim$0.3 V.

The potential of oxygen electrodes is known to be difficult to control. At a fixed current density, the potential may shift by as much as 0.3 V. Any shift at the oxygen electrode would also affect the reduction potential if the electrolysis were controlled by using a fixed potential between the anode and the cathode. To avoid these shifts, a potentiostatic control may be necessary,** even on a process scale.

The electrode reaction on the counter electrode during reoxidation is

$$H^+ + e^- \rightleftarrows 1/2\ H_2 \qquad E^\circ = 0$$

It is the most studied and best known of all electrochemical reactions, having overvoltages ranging from less than 0.1 V to more than 1.5 V for various electrode materials.

If electrolysis is applied in the partitioning step of the first cycle of a Purex process, uranyl ions would be reduced in addition to Pu(IV). The partial reduction of uranyl ions is desirable because uranous nitrate is a chemical reductant for Pu(IV); i.e.,

$$U^{4+} + 2\ Pu^{4+} + 2\ H_2O \rightarrow UO_2^{2+} + 2\ Pu^{3+} + 4\ H^+$$

---

* The sign convention for electrode reactions has changed twice in the past two decades. Cohen used the thermodynamic convention, expressing the oxygen-discharge electrode with a negative potential respective to hydrogen. In this article, the potentials are given the polarities measured, i.e., the oxygen potential is positive with respect to hydrogen.

** A potentiostat maintains a fixed potential of the working electrode relative to a stable reference electrode.

Any electrolytically reduced uranyl ion acts as a chemical reductant for Pu^{4+}, regenerating the uranyl and adding to the electrolytic alloy reduced plutonium. Since uranyl ions are present in large excess in the partitioning step (particularly at the plutonium-lean end of the partitioning bank), a dramatic improvement in the rate of the overall plutonium reduction is achieved by this catalytic action. The complete electrode reaction for the reduction of uranyl ions is:

$$UO_2^{2+} + 4\ H^+ + 2e^- \rightleftarrows U^{4+} + 2\ H_2O \qquad E^\circ = +0.334$$

The overpotential for reducing uranyl ion may be ~0.3 V or higher, since the reaction is partly irreversible. The reduction of uranyl ion, therefore, proceeds near the equilibrium potential for hydrogen, and hence hydrogen evolution could occur simultaneously with the reduction of uranyl ions. Hydrogen evolution can be prevented by using a cathode material with a high hydrogen overpotential. In many preparatory processes for uranous nitrate production, this is indeed done.[7,17-19] However, in Purex processes, significant quantities of air are entrained in the liquid streams and the medium is oxidizing. If the electrode material is oxidized, it may become inactive. Mercury is easily oxidized and hence is not suitable. The choice of electrode material in the partitioning step is likely to be more difficult than for the isolation part of the flowsheet because hydrogen evolution must be avoided.

C. Process Application

The important process considerations that must be met in fitting the electrolytic step into the process are as follows:

1. The electrolytic cells must be integrated with centrifugal contactors.
2. Reduction rate must be adequate.
3. Interference from other electrochemical reactions must be insignificant.

The first two problems are evaluated in the next two sections.

1. Integration of the Electrolytic Process

In the stripping step of a typical Purex plutonium cycle, the organic stream containing the tetravalent plutonium is contacted countercurrently with the aqueous reducing (stripping) solution containing ferrous sulfamate. The reductant is only slightly soluble in the organic phase, and reduction occurs mostly in the aqueous phase between ferrous ion and the Pu(IV), which is continuously extracted from the organic phase. If an electrolytic method were to be used instead of ferrous ions in a mixed two-phase system, electrodes must be incorporated with the mixing equipment. This approach has indeed been taken in development work at Karlsruhe.

In future Purex processes for LMFBR fuels, extractors will be used that minimize residence time, minimizing also the radiolytic decomposition of the organic stream. The most promising extractors for this application are centrifugal contactors. The direct incorporation of electrodes into centrifugal contactors would add considerable complexity to their design,

and it appears likely that residence times in a centrifugal contactor would be too short for adequate reduction of plutonium. Accordingly, alternative modes of integrating electrolysis into the process were considered.

A conceptual scheme (see Fig. V-2) uses a multistage bank of centrifugal contactors. Dilute nitric acid (stripping solution) is fed into the plutonium-lean end of the multistage unit. Because of the favorable distribution coefficient, some of the residual Pu(IV) from the organic stream back-extracts into the aqueous phase. Conditions (flow rates and acidity) are set so that the plutonium level in the exiting organic stream is at an acceptably low level.

The aqueous stream from this first mixing stage is passed through an electrolytic cell where the Pu(IV) is reduced to Pu(III); reduction need not be complete, as is discussed below. The aqueous stream then enters the next stage and contacts the countercurrently flowing organic stream. The Pu(IV) content of the organic phase is higher than that of the entering aqueous phase and so Pu(IV) partially backextracts into the aqueous phase; meanwhile, the Pu(III) in the aqueous phase is retained. The aqueous stream, now richer in plutonium, passes into a second electrolytic cell, and again the Pu(IV) is reduced. This procedure is repeated to the extent necessary. The aqueous product stream from the last stage contains mainly Pu(III). Hydrazine can be added as a stabilizer if needed.

Aspects of this concept can be further elaborated. First, 100% reduction of Pu(IV) to Pu(III) in a given cell is not necessary but only reduction to a level such that additional stripping of plutonium is accomplished in the next contactor. The number of required stages is inversely related to the extent of plutonium reduction in a stage. Reduction requirements for a given cell are related to the degree of polymerization of Pu(IV)[20] which, in turn, is a function of acidity and temperature; polymer formation is enhanced at low acidities and high temperatures. In the present concept, the unit would operate at acidities above the minimum acidity for polymer formation.

In the conceptual scheme, the electrolytic reduction cell is separated from the contactor proper, avoiding undue complication of the contactor design and allowing flexibility in cell design (electrode size, electrode spacing, and residence time) and convenient maintenance. This approach would also permit use of a concentrated (30%) TBP flowsheet and would provide high throughput and a concentrated plutonium product stream. Criticality safety would be accomplished by means of critically safe geometry of the contactor and the electrolytic cells.

To illustrate the concept with an example, an idealized material balance flowsheet was calculated. An organic feed stream, containing about 50 g Pu(IV) per liter would be countercurrently extracted with 0.4M nitric acid. Flow rates were taken to be equal. The distribution coefficient for this system would be 0.33 (at 19% TBP in kerosene).[21] Electrolysis would be carried out between each pair of extraction stages and was assumed to be 75% complete in each stage (reduction of 75% of the Pu(IV) is a conservative estimate, see Section 2d). Under these conditions, 99.9% extraction would be reached in five stages. The product stream would

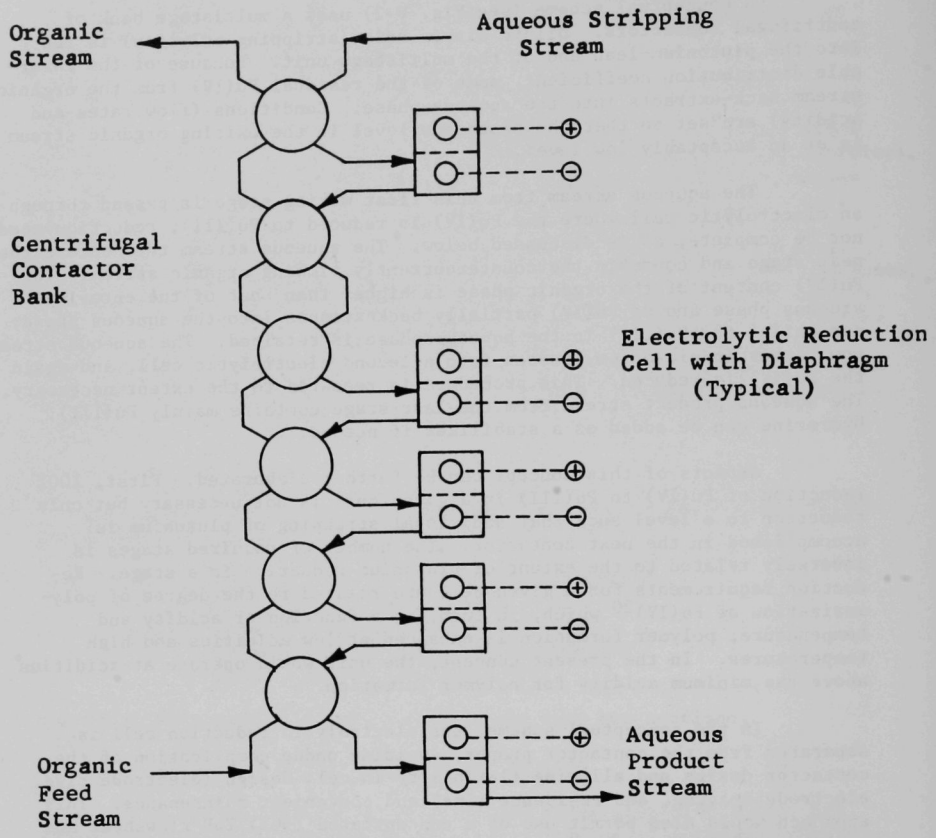

Fig. V-2. Conceptual Scheme for Electrolytic Plutonium Valence Adjustment with Centrifugal Contactors

contain 80% Pu(III) and 20% Pu(IV). In practice, some nitric acid would also be extracted from the organic stream. As a result, acidities would increase and distribution coefficients decrease, necessitating a sixth stage.

2. Reduction Rate

In every electrolytic process, the rate of electrolysis is proportional to the current. The size of an electrolytic cell is determined from the ratio of attainable current to electrode area (i.e., the current density), and the desired reduction rate. The size of electrolytic cells should be comparable to the size of other process equipment, but the reduction rate has to match the flow rate of the process streams. This requirement is defined in terms of the magnitude of the current density attainable in a reduction cell under Purex conditions. Factors which influence current density and which can also be manipulated in an on-stream electrolysis are electrolyte agitation, electrode geometry, and cell design.

a. Current Densities

Current flows from an electrode into an electrolyte in three consecutive steps: (1) the ion being electrolyzed is transported to the electrode, (2) an electron is transferred between the ion and the electrode, (3) the reaction products are removed from the electrode. The first and third steps are mass transport phenomena and relate to three transport mechanisms: diffusion, migration, and convection. The second step is an electrochemical reaction. Its rate is usually fast, if the reaction is reversible, as is the case for $Pu^{4+} + e^- \rightleftarrows Pu^{3+}$.[16] The magnitude of the current density is thus mass transport-dependent and is dependent on the rates of diffusion, migration, and convection. Diffusion describes the motion of ions under the influence of a concentration gradient, migration occurs in electric fields, and convection is caused by mechanical forces on the bulk solution.

In agitated solutions, an equilibrium steady state is reached between the three transport mechanisms. Efforts to calculate the steady state from hydrodynamic principles have led Levich to the equation:[22]

$$Nu = A\ Re^m\ Sc^n \qquad (1)$$

where Nu is the Nusselt number; Re, the Reynolds number; Sc the Schmidt number; and A, m, and n are constants.

For electrochemical processes, the Nusselt number Nu is defined[23] as

$$Nu = \frac{i\ D\ (1 - T)}{NF\ D_{jk}\ (C_\infty - C_o)}$$

[i = current density (A/cm^2); D = characteristic electrode dimension (cm); T = transport number (dimensionless); N = equivalents per mole (equiv/mol); F = Faraday constant (A-sec/equiv); D_{jk} = diffusion coefficient of electrolyzed ion in electric fields (different from molecular diffisuion coefficient) (cm^2/sec); C_∞ = concentration in bulk solution (mol/cm^3); C_o = concentration on electrode surface (mol/cm^3)]. The Reynolds number is

$$Re = \frac{Dv}{\nu}$$

[v = linear flow velocity (cm/sec); ν= kinematic viscosity (cm^2/sec)]. The Schmidt number is

$$Sc = \frac{\nu}{D_{jk}}$$

In deriving Eq. 1, laminar flow was assumed and boundary layer theory was used. The constants A, m, and n depend on the geometry of the electrode, but some generalizations can be made. For flat plates in parallel laminar flow, numerical values for A, m, and n have been calculated.[22,24]

$$A = 0.67 \qquad m = 1/2 \qquad n = 1/3$$

A slightly different value for A of 0.66 was given by Wranglén.[25] Trümpler et al.[26] measured m experimentally for plates in parallel flow and obtained a value of 0.43 instead of 0.5. However, their electrodes were cylindrical rather than flat. The exponent n of the Schmidt number has been confirmed in numerous studies[27] and is always given as 1/3.

For cylindrical electrodes in transverse flow, the mass transport is complicated by the fact that the boundary layers separate at Reynolds numbers higher than one. Thus, Levich's assumption of laminar flow is not strictly valid. Nevertheless, Cairns et al. demonstrated experimentally that m = 1/2 and n = 1/3 are still valid at Reynolds numbers between 100 and 3000.[28] The coefficient A could not be measured accurately in Cairn's experiment. Because of the equivalence of heat and mass transport (see Section D below), a value of 0.6 was suggested. Thus, the transport of ions to an electrode can be described over the flow range $100 < Re < 2000$ by the same simple equation for the most common geometries of both plates and cylinders:

$$Nu = A\, Re^{1/2}\, Sc^{1/3} \tag{2}$$

For plates, A is 0.67; for cylinders, A is 0.60.

At lower and higher Reynolds numbers, different values for A and m have to be used. In Section D below, Johnson has shown that for cylindrical electrodes in transverse flow at low Reynolds number, A = 0.9 and m = 0.4. At Reynolds numbers higher than 2000, m becomes larger than 1/2,[29] and the mass transport rate will generally increase (see also Fig. V-4 in Section D).

By substituting the variables for the dimensionless groups, Eq. 2 becomes:

$$i = \frac{A\, NF\, D_{jk}^{2/3}\, \nu^{1/2}\, (C_\infty - C_o)}{(1 - T)\, D^{1/2}\, \nu^{1/6}} \tag{3}$$

Equation 3 shows that the rate of mass transport per unit area, or the current density, is proportional to the concentration gradient $C_\infty - C_o$ between the bulk solution and electrode surface. When C_o becomes zero, the current density reaches an upper limit and is called the limiting current density:

$$i_L = \frac{A\ NF\ D_{jk}^{2/3}\ \nu^{1/2}\ C_\infty}{(1 - T)\ D^{1/2}\ \nu^{1/6}} \qquad (4)$$

To reach the limiting current density, a sufficiently large potential has to be applied to the electrode. In practice, a voltage versus current curve is measured to determine the potential.

Equation 4 shows how the magnitude of the limiting current density can be influenced. For a given electrolyte such as the Pu(IV)-HNO_3 stream of a Purex process, N, F, D_{jk}, T, ν and C_∞ are fixed. D, A, and v depend on the shape of the electrode and the cell design and can be manipulated. Increased flow velocity, small characteristic electrode dimension, and favorable electrode geometry will increase the current density.

The characteristic electrode dimension D is the diameter of the cylinder for cylindrical electrodes in transverse flow and the length of the plate for flat plates in parallel flow.[24] As an illustration of the effect of D on i_L, the limiting current density has been calculated for two wires of 0.019-cm and 0.051-cm diameter (typical for 60 and 14 mesh screen) and for a 0.5-cm long plate. The electrolyte was taken as a 0.1M Pu(IV) solution in 0.5M HNO_3, flowing with a velocity of 20 cm/sec. The transport number T is not known, but was taken as 0.1 for all three electrodes. The value of A was 0.67 for the plate and 0.6 for the wire; D_{jk} is 5.8×10^{-6} cm^2/sec.[16] Since ν is again not known for Pu(IV) solutions, the value of 9×10^{-3} cm^2/sec at 25°C for a similar uranyl nitrate solution was used instead.[30] The limiting current densities (mA/cm^2) were as follows: 148 for 0.051-cm-dia wire, 90 for 0.051-cm-dia wire, and 29 for 0.5-cm-long plate. Thus, higher current densities are obtained with thin wire electrodes.

b. Residence Times

The preceding discussion led to an equation between limiting current density and several variables, characterizing the electrolyte and the electrode. Equation 4 and Faraday's law can be combined to calculate the amount of material reduced per unit time in an electrolytic cell. The dimensions of a cell in which this quantity of material could be reduced can also be determined from Eq. 4 and the plutonium concentration. The calculation is complicated by the fact that the Pu(IV) concentration and hence the current will change during electrolysis. Thus, Faraday's law has to be written for a variable current:

$$\Delta M = \frac{\int I\ dt}{NF} \qquad (5)$$

ΔM is the number of moles being reduced, I is the current, and N and F have the usual meanings. Dividing Eq. 5 by the electrolyte volume, V introduces concentrations into Faraday's law:

$$\frac{\Delta M}{V} = C_i - C = \frac{\int I \, dt}{NFV} \tag{6}$$

where V is the cell volume, C_i is the concentration at the beginning of the electrolysis, and C is the concentration at time t. The rate of reduction is the time derivative:

$$\frac{dC}{dt} = - \frac{I}{NFV}$$

Substituting the current density of Eq. 4, multiplied by the surface area S of the electrode, for I in Eq. 6 gives

$$\frac{dC}{dt} = - \frac{A \, D_{jk}^{2/3} \, \nu^{1/2} \, S \, C_\infty}{(1 - T) \, D^{1/2} \, \nu^{1/6} \, V} \tag{7}$$

Equation 7 illustrates the proportionality between reduction rate and concentration. A reduction constant, ε, is defined here for substitution in Eq. 7.

$$\varepsilon = \frac{A \, D_{jk}^{2/3} \, \nu^{1/2} \, S}{(1 - T) \, D^{1/2} \, \nu^{1/6} \, V} \tag{8}$$

Integration then gives

$$\ln C + a = -\varepsilon t + b$$

The two integration constants are obtained from the first boundary condition that C be equal to C_i at t = 0. Thus

$$\ln C_i = b - a$$

$$\ln C - \ln C_i = -\varepsilon t \tag{9}$$

Equation 9 describes the concentration of Pu(IV) in a volume element of electrolyte after it enters the cell and while passing through it. The concentration decreases exponentially with time. Examining epsilon reveals that it contains four groups of variables. D_{jk}, T, and ν are properties of the electrolyte, A and D relate to the configuration of the electrode, S and V are cell design parameters, and v is an operational parameter. In a given cell, the flow velocity v is related to the time t the electrolyte is in the cell. This residence time is important for the practical process operation.

Setting $C = 1/2\ C_i$ in Eq. 9 gives the time required to reduce one-half of the initial plutonium:

$$t_{1/2} = \frac{\ln 2}{\varepsilon} \tag{10}$$

This "half reduction time" is independent of concentration. Since the initial Pu(IV) concentrations will vary at different reduction points in the process, it would be advantageous to design the reduction cell as a module with a residence time equal to the "half reduction time." The number of modules in series to achieve a desired percentage of reduction could then be read from the following tabulation:

number of modules	percent reduction
1	50
2	75
3	88
5	97

In practice, a residence time of less than one minute would be desirable to minimize holdup in the equipment. In a following section, the "half reduction time" of a conceptualized cell is calculated.

c. Reduction Cell Effectiveness

A comparison between different cell designs and their relative effectiveness cannot be made on the basis of absolute reduction rates because rates depend also on concentrations. The effectiveness of a cell can be measured by the ratio of reduction rate to concentration. We define:

$$\text{effectiveness} = \frac{-\frac{dC}{dt}}{C_\infty} \tag{11}$$

The rate $\frac{dC}{dt}$ can be substituted from equations 7 and 8

$$\text{effectiveness} = \frac{\varepsilon C_\infty}{C_\infty} = \varepsilon$$

Thus we find that the previously introduced reduction constant ε can be used as a measure of the cell effectiveness. In contrast to the radioactive decay constant, cell effectiveness is a property of the total reduction system, including the cell, the electrodes, and the electrolyte, and of operational parameters such as the flow velocity.

d. Pressure Drop in a Reduction Cell

Equation 8 shows that the effectiveness of a cell can be improved in three ways. First, by making the ratio of electrode surface to cell volume high, second, by a small characteristic dimension, D, of the electrode, and third, by a high linear flow velocity. Modifications in

accord with the second and third principles are equally effective, but each will cause an increased pressure drop across the cell.

If electrolytic cells are interposed between centrifugal contactors as shown in Fig. V-2, the pressure represented by the pumping force of the fast contactors (which is not very large) must exceed the pressure drop in the cells. Hence, the pressure drop must be carefully considered when designing a reduction cell. In fuel-cell development, where high current density is an important goal, flow-through electrodes (especially porous metals) were found effective.[23] On the other hand, porous metals cause a large pressure drop because the liquid is forced through narrow channels. As a compromise, flow-through electrodes with wider flow channels, such as wire cloth or metal grates, have been considered. If a reduction cell is to have a uniform current density, the wire cloth cathode should be located symmetrically between two anodes and separated from the anodes by two diaphragms. A schematic drawing of such a conceptualized cell is shown in Fig. V-3. The electrolyte flows through the channel between the two diaphragms but is forced back and forth through the cathode by baffles.

The pressure drop across such a cell would mainly consist of two terms: $n\ \Delta P_E$, the pressure drop across one layer of wire cloth multiplied by the number of passes, and $n\ \Delta P_B$ the pressure drop when the liquid flows around a baffle multiplied by the number of baffles.*

$$\Delta P_{total} = n\Delta P_E + n\Delta P_B \tag{12}$$

ΔP_E and ΔP_B were calculated by Johnson (Section E below).

$$\Delta P_E = 1.5M\ (2\text{-}MD)\ (\rho v^{0.15})(D^{0.85}\ v^{1.85}) \tag{13}$$

$$\Delta P_B = \rho v^2\ (\frac{H}{L_B})^2 \tag{14}$$

where ρ is the density of the electrolyte, H is the distance between baffles, and L_B is the width of the baffle opening.

Equation 13 can be simplified if the most common type of wire cloth, called market grade, is used as electrodes. Table V-1 gives some dimensions of these cloths. The ratio of the projected area of the wires to the flow area, MD (2-MD), see Section E below, for these cloths can be approximated by 1.6 MD, and M can be expressed as a function of D:

$$M = 0.064\ D^{-3/2}$$

When substituted into equation 13, the pressure drop for one layer of wire cloth becomes:

$$\Delta P_E = \frac{0.15\rho\ v^{0.15}\ v^{1.85}}{D^{0.65}} \tag{15}$$

*The pressure drop due to flow in the channel, ΔP_C, was small compared to pressure drops due to the electrode and the baffle.

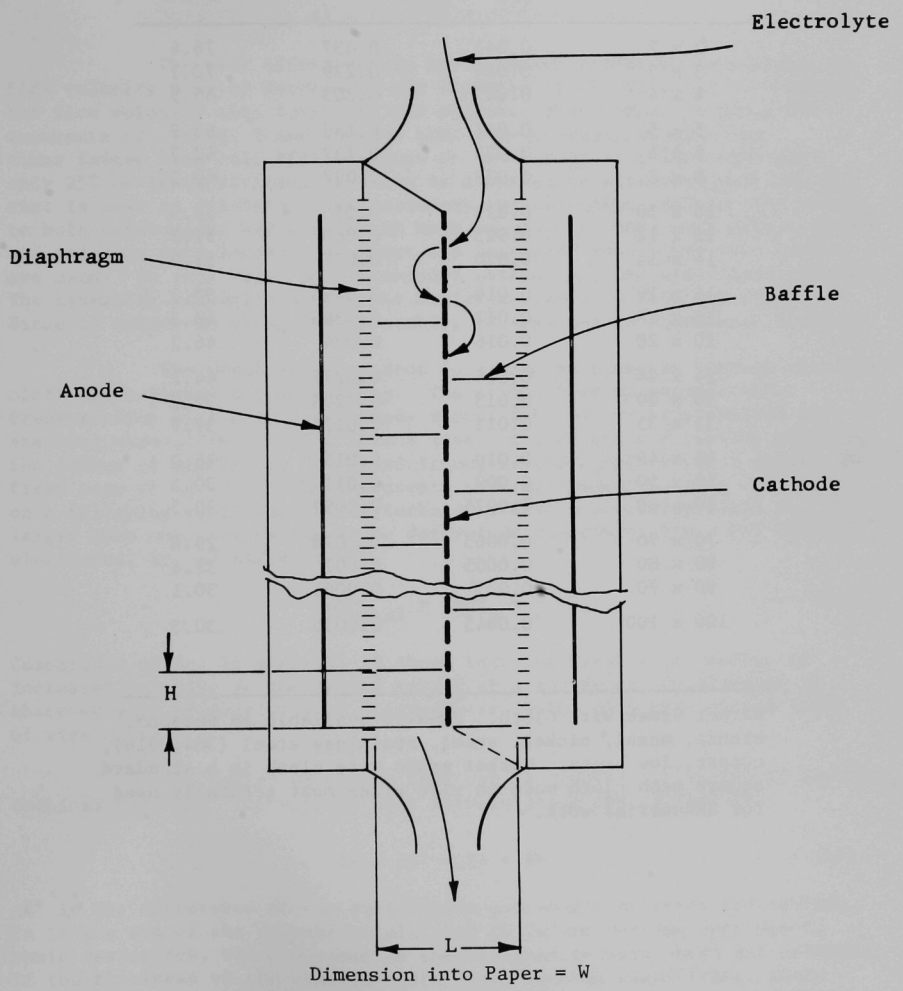

Fig. V-3. Schematic Drawing of Reduction Cell
(H = separation of baffles; L = width of channel)

TABLE V-1. Dimensions of Market-grade Wire Cloth[a]

Meshes Per Linear Inch	Diameter of Wire, in.	Width of Opening, in.	Open Area, Percent
2 x 2	0.063	0.437	76.4
3 x 3	0.054	0.279	70.1
4 x 4	0.047	0.203	65.9
5 x 5	0.041	0.159	63.2
6 x 6	0.035	0.132	62.7
8 x 8	0.028	0.097	60.2
10 x 10	0.025	0.075	56.3
12 x 12	0.023	0.060	51.8
14 x 14	0.020	0.051	51.0
16 x 16	0.018	0.0445	50.7
18 x 18	0.017	0.0386	48.3
20 x 20	0.016	0.034	46.2
24 x 24	0.014	0.0277	44.2
30 x 30	0.013	0.0203	37.1
35 x 35	0.011	0.0176	37.9
40 x 40	0.010	0.015	36.0
50 x 50	0.009	0.011	30.3
60 x 60	0.0075	0.0092	30.5
70 x 70	0.0065	0.0078	29.8
80 x 80	0.0055	0.007	31.4
90 x 90	0.005	0.0061	30.1
100 x 100	0.0045	0.0055	30.3

[a]Market Grade Wire Cloth. Usually available in phosphor bronze, monel, nickel, steel, stainless steel (304, 316), copper, low brass. Market grade wire cloth is a standard square mesh cloth made in wire sizes most generally used for industrial work.

Equation 15 contains some of the same independent variables as Eq. 8, which defined the cell effectiveness. By comparing these, a critical judgment can be made on how the pressure drop can be most effectively used to improve the cell effectiveness. For ease of comparison, Eq. 8 is repeated here:

$$\varepsilon = \frac{A\, D_{jk}^{2/3}\, S\, v^{1/2}}{(1 - T)\, \nu^{1/6}\, V\, D^{1/2}} \tag{8}$$

The cell effectiveness is increased either by increasing the flow velocity v or by decreasing the diameter of the wire, D. Increasing the flow velocity also increases the pressure drop, ΔP_E. In fact, the exponents of ν in Eq. 8 and 15 show that ΔP_E increases almost four times faster than cell effectiveness or (expressed in a different way) only 25% of the additional pressure is absorbed by mass transport and the rest is lost in friction. The exponents for the other variable (D) common to both expressions are similar in both equations. Thus both effectiveness and pressure drop increase at about the same rate when finer wire cloths are used. In this case, mass transport absorbs all the additional pressure. The kinematic viscosity is another variable common to both equations. Since it cannot be changed appreciably, it need not be considered further.

The total pressure drop is caused by n passes through the wire cloth and n passes around baffles. The second term is unproductive. Pressure drop as a result of passes around baffles can be minimized by stacking wire-cloth cathodes into a layer of k cloths and thereby reducing the number of baffles to $\frac{n}{k}$. In addition, an empirical factor α enters the first term of Eq. 12. Alpha represents the improvement in mass transport on a following cloth due to the turbulence from a preceding cloth and is larger than one. Alpha has to be determined experimentally. For stacked electrodes, Eq. 12 becomes:

$$\Delta P_{total} = \alpha n \Delta P_E + \frac{n}{k} \Delta P_B \tag{16}$$

Comparison of Eq. 16 with Eq. 12 shows that the first term, $\alpha n \Delta P_E$, is increased relative to the second term $\frac{n}{k} \Delta P_B$, and hence the pressure is absorbed more productively by stacked wire cloths than by a single layer of wire cloth.

The number of cloths that can be stacked is limited by electrochemical factors. The voltage drop between anode and cathode is:

$$\Delta E = \Delta E^\circ + \Sigma\eta + IR \tag{17}$$

ΔE° is the difference of the equilibrium potentials at anode and cathode, $\Sigma\eta$ is the sum of the overpotentials, and IR is the voltage drop due to ohmic resistance, which depends on the distance between anode and cathode. If the thickness of the stacked-cloth layer becomes significant, there would be a shorter distance between the anode and the outer cathode layers than between the inner cathode layers and the anode. As a result, the resistance between the anode and the various layers of the cathode would vary.

Since the total voltage difference, ΔE, between anode and the various cathode layers would be the same, according to Eq. 17 the current I would have to vary. A larger current would flow through the outer than through the inner cathode layers. The consequence would be a loss in effectiveness. If the current on the inner layers should be increased by increasing ΔE, hydrogen would evolve at the outer layers.

It is difficult at this stage to decide what percentage of the cathode-anode separation is acceptable as cathode thickness, but 20% appears conservative.

In summary, the design principles are:

1. The electrode surface to electrolyte volume ratio should be as high as possible.
2. The wire in the wire cloth cathode should be as fine as practical.
3. The flow velocity should be as high as the pressure drop permits.
4. Wire cloth should be stacked but not beyond a thickness equal to 20% of the cathode-anode separation.

These principles are applied in the following discussion to the specification of dimensions for the conceptualized cell in Fig. V-3. The pressure drop and the "half reduction time" are then calculated for the specified cell.

We start by selecting the mesh size of the cathode. In a practical process, it may be desirable to allow small particles to pass through the cloth, but for effectiveness, a fine screen is necessary. In the present case, a 60-mesh market-grade wire cloth was selected (see Table V-1). Such a cloth has a thickness of 0.04 cm. Stacking ten cloths into a layer at 0.04-cm separation results in a cathode thickness of 0.04 x 19 = 0.76 cm. For the cathode thickness to be 10% of the cathode-anode separation, the separation must be 7.6 cm. Next, the positions of the diaphragms have to be chosen. Somewhat arbitrarily, we place diaphragms 5 cm from the center of the cathode on each side. Thus we have fixed the magnitude of L_B. For convenience in calculating ΔP_B, we set H, the separation of the baffles, to be equal to L_B. The pressure drop of such a cell can be calculated from Eq. 16, using Eqs. 14 and 15 for ΔP_B and ΔP_E. For ρ, the density of 0.1M $UO_2(NO_3)_4$ in 0.5M HNO_3 is used[28] (1.18 g/cm^3). Alpha is somewhat freely estimated to be 1.5. Thus

$$\Delta P_{total} = n\ 1.5\ \frac{0.15 \cdot 1.18 \cdot 0.5 \cdot v^{1.85}}{0.075} + \frac{n\ 1.18\ v^2}{10}$$

$$= 1.77\ n\ v^{1.85} + 0.118\ n\ v^2$$

A centrifugal contactor is capable of providing a pressure equivalent of at least 2 ft of water or 5.9×10^4 dyn/cm^2. At a flow velocity of 20 cm/sec, the number of passes in a cell that would cause this pressure loss is

$$n\,(1.77\,v^{1.85} + 0.118\,v^{2}) = 5.9 \times 10^{4}$$

$$n = 118$$

The "half reduction time" is calculated from the surface-to-volume (S/V) ratio of the described cell. A 60-mesh wire cloth has a wire surface area of 2.82 cm^2/cm^2 of cloth; 10 wire cloths in a cathode compartment of 10-cm thickness gives (S/V) = 2.82. If values assigned to the variables in the text are put in Eq. 8, the effectiveness becomes

$$\varepsilon = \frac{0.6 \cdot 3.25 \cdot 10^{-4} \cdot 2.82 \cdot v^{0.5}}{0.9 \cdot 0.46 \cdot 0.137}$$

$$= 9.7 \times 10^{-3}\, v^{0.5}$$

at a flow velocity of 20 cm/sec

$$\varepsilon = 4.4 \times 10^{-2}$$

The "half reduction time," $t_{1/2}$, is

$$t_{1/2} = \frac{\ln 2}{\varepsilon} = 16 \text{ sec}$$

A "half reduction time" of 16 sec is acceptable from the standpoint of holdup in the process. In only 32 sec, the 75% reduction used in the material balance calculation would be reached. A cell for 32-sec residence time would have approximately 90 baffles and hence would have a low enough pressure drop.

The flow velocity chosen in this model calculation may have been too high; at a flow velocity of 20 cm/sec, attaining a residence time of 32 sec would require a rather long cell. However, the same effectiveness can be reached at only one-tenth this flow velocity if the S/V ratio is increased by a factor of 3.2. Such a cell would be about 45 cm long in the direction of flow and would be slab-shaped for criticality reasons. The width of the slab at a volume flow rate of 2 gal/min would be about 20 cm. These dimensions are of the same magnitude as those of proposed centrifugal contactors (see Section C.1 above), showing that an adequate reduction rate is feasible in small enough cells.

D. Mass Transfer from Cylinders (Terry Johnson)

Only a small amount of data exist on the mass transfer from single cylinders to liquids at low Reynolds numbers. Because the j factor for mass transfer equals the j factor for heat transfer, the large body of heat transfer data from single cylinders can be employed to estimate mass transfer rates.[31] There is an analogy between heat and mass transfer because both heat and mass are transferred from the solid surface to the

bulk fluid through similar boundary layers. The boundary layer around a bluff body such as a cylinder is complicated by the separation of the layer from the solid surface and the formation of a turbulent wake behind the cylinder. Because of the character of this boundary layer around a cylinder, it is not possible to represent the Nusselt or Sherwood numbers as simple functions of the Reynolds number over a wide range of flow conditions. This is demonstrated by a large amount of data for heat transfer in air as shown by Fig. V-4 taken from McAdams.[32] The relationship:

$$Nu = 0.6\ Re^{1/2}\ Pr^{1/3},$$

where Pr is the Prandtl number, which is commonly used to represent heat transfer from cylinders, does fit the data in the range of Re from 10^2 to 10^4. However, at Re = 1.0, the heat transfer coefficient is underestimated by 40%. At low Reynolds numbers, the heat transfer data were approximated by a two-constant equation

$$Nu = 0.825\ Re^{0.4} \qquad (1 < Re < 200)$$

(see Fig. V-4). Recommendations of several authors[33,34] are that heat transfer to liquids can be represented by:

$$Nu = [0.825(Re)^{0.4}] \cdot [1.1\ Pr^{1/3}].$$

By use of the analogy between heat and mass transfer, the above equation was applied to mass transfer by replacing the Nusselt and Prandtl numbers by the Sherwood and Schmidt numbers, Sh and Sc. The equation thus becomes

$$Sh = 0.907\ Re^{0.4}\ Sc^{1/3}$$

E. Pressure Drop in an Electrolytic Cell (Terry Johnson)

The total pressure drop (ΔP_{total}) in the fluid flowing through one cell of the type shown in Fig. V-3 is the sum of the pressure drops due to flow over the electrode (ΔP_E), through the channel (ΔP_C), and around the baffle (ΔP_B). Where the size of the flow channel is uniform, the pressure drop due to velocity changes will be negligible compared to the other losses.

$$\Delta P_{total} = \Delta P_E + \Delta P_C + \Delta P_B$$

The pressure drop across an electrode that consists of a screen or a stack of screens was estimated as the total force, F, of the fluid on the cylindrical wires of the screen. The pressure drop across one layer of a screen electrode is

$$\Delta P_E = \frac{F}{A_F} . \qquad (18)$$

where A_F is the fluid flow area in the channel. The drag coefficient, C_D, is defined by

$$C_D = \frac{2F}{A_p\ \rho v_E^2} \qquad (19)$$

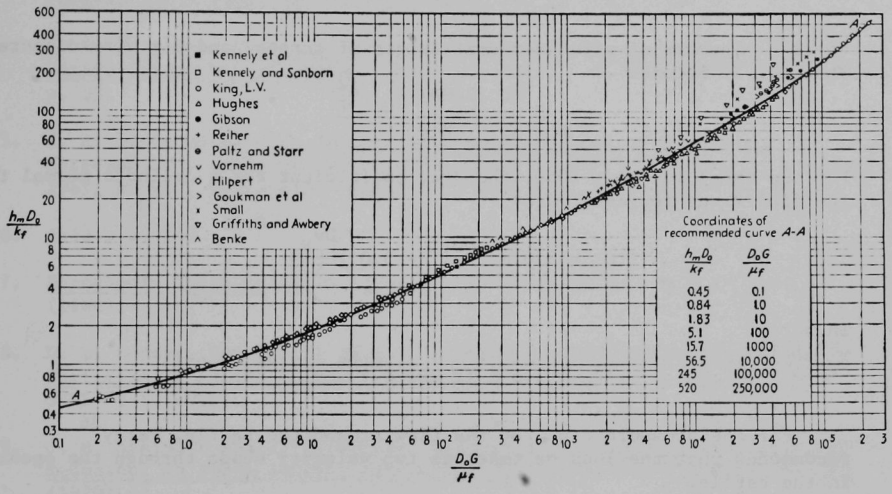

Fig. V-4. Data for Heating and Cooling Air Flowing Normal to Single Cylinders, Corrected for Radiation to Surroundings. From Heat Transmission by William H. McAdams, copyright by William H. McAdams, 1954. Used by permission of McGraw-Hill Book Company.

where A_p = projected area of the wire cloth, ρ = density of fluid, and v_E = fluid velocity over the electrode. Then

$$\Delta P_E = \frac{C_D A_p \rho v_E^2}{2 A_F} \tag{20}$$

The ratio of the projected area of the wires of the screen to the total fluid flow area is

$$\frac{A_p}{A_F} = MD\ (2\text{-}MD) \tag{21}$$

where M = number of wires per unit length of screen, and D = wire diameter. Thus Eq. 20 becomes

$$\Delta P_E = \frac{MD\ (2\text{-}MD)\ C_D\ \rho v_E^2}{2}$$

For the range $1 < Re < 2000$, the drag coefficient for a cylinder normal to the flow[35] was represented by

$$C_D = 3.0\ Re^{-0.15} = 3.0\ [\frac{Dv_E}{\nu}]^{-0.15}$$

Thus

$$\Delta P_E = 1.5\ M\ (2\text{-}MD)\ D^{0.85}\ v_E^{1.85}\ \rho\nu^{0.15}$$

For the pressure drop for the flow around the baffle, Perry[36] recommends that the loss be taken as two velocity heads through the opening in the baffle.

$$\Delta P_B = 2\ \rho v_B^2$$

The flow velocity around the baffle, v_B, is

$$v_B = v_C \frac{H}{L_B}$$

where v_C is the flow velocity in the channel (see Fig. V-3). Thus the pressure drop around the baffle becomes

$$\Delta P_B = \rho v_C^2 (\frac{H}{L_B})^2$$

The pressure drop due to flow in the channel will be small compared with pressure drops due to the electrode and the baffle. Thus the total pressure drop is estimated to be

$$\Delta P_{total} = 1.5M\ (2\text{-}MD)\ D^{0.85}\ V_E^{1.85}\ \rho\nu^{0.15} + \rho v_C^2\ (\frac{H}{L_B})^2$$

REFERENCES

1. E. R. Irish, Description of Purex Plant Process, USAEC report HW-60116 (May 19, 1959).

2. W. E. Unger, R. E. Blanco, C. D. Watson, D. J. Crouse, and A. R. Irvine (comps.), Aqueous Processing of LMFBR Fuels, Progress Report No. 1, March 1969, USAEC report ORNL-TM-2552, and subsequent reports in this series.

3. Aqueous Processing of LMFBR Fuels - Technical Assessment and Experimental Program Definition, pp. 369-383, USAEC report ORNL-4436.

4. D. E. Ferguson, Chemical Technology Division Annual Progress Report for Period Ending May 31, 1968, (September 1968). USAEC report ORNL-4272, p. 50.

5. H. A. C. McKay et al., Solvent Extraction Chemistry of Metals, International Conf. on Solvent Extraction Chemistry of Metals, Harwell, 1965, p. 117, Macmillan, New York (1965).

6. ibid., p. 103.

7. Eurochemic Third Activity Report, 1964-1966, report NP-17623, p. 77 (1966).

8. D. E. Horner, The Use of Ferrous Nitrate as a Plutonium Reductant for Partitioning Plutonium and Uranium in Purex Processes, USAEC report ORNL-4383 (1969).

9. J. M. McKibber and J. E. Bercaw, Hydroxylamine Nitrate as a Plutonium Reductant in Purex Solvent Extraction Processes, USAEC report DP-1248 (1970).

10. LMFBR Fuel Cycle Studies Progress Report for January 1970, No. 11, USAEC report ORNL-TM-2871, p. 21.

11. E. K. Dukes, J. Am. Chem. Soc., 82, 9 (1960).

12. G. Koch, W. Ochsenfeld, and E. Schwind, Flowsheet Studies on Processing of Plutonium Fuels by Solvent Extraction, report KFK-990 (May 1969).

13. B. F. Roth and W. Roos, Design of an Electrolysis Cell and Plan of a Test Stand for Direct Reduction of Pu(IV), report NP-18167 (December 1969).

14. D. Cohen, J. Inorg. Nucl. Chem. 18, 207 (1961).

15. A. G. Wain, The Potential of the Pu(III)-Pu(IV) Couple in Nitric Acid Solution, report AERE-R-5320 (1966).

16. D. G. Peters and W. D. Shults, J. Electroanal. Chem. 8, 200 (1964).

17. M. B. Finlayson and J. A. S. Mowat, Electrochem. Technol. 3, 148 (1965).

18. N. Parkinson, J. A. S. Mowat, and M. B. Finlayson, Electrolytic Reduction for Solutions Containing Nuclear Fuel, Brit. Pat. 1,096,592 (1967).

19. G. S. Nichols, Electrolytic Preparation of Uranous Nitrate, USAEC report DP-1065 (1966).

20. S. Mann and A. R. Irvine, A Study of Plutonium Polymer Formation and Precipitation as Applied to LMFBR Fuel Reprocessing, USAEC report ORNL-TM-2806 (1969).

21. L. L. Smith, Solvent Extraction Data for Plutonium, USAEC report DP-700 (1962).

22. V. G. Levich, Physicochemical Hydrodynamics, Prentice-Hall, Englewood Cliffs, N. J. (1962).

23. H. A. Liebhafsky and E. J. Cairns, Fuel Cells and Fuel Batteries, p. 237 John Wiley, New York (1968).

24. V. G. Levich, Discuss. Faraday Soc. 1, 37 (1947).

25. G. Wranglén, Acta. Chim. Scand. 13, 830 (1959).

26. G. Trümpler and H. Zeller, Helv. Chim. Acta. 34, 952 (1951).

27. R. B. Bird, W. E. Steward, and E. N. Lightfoot, Transport Phenomena, p. 605, John Wiley, New York (1970).

28. E. J. Cairns and A. M. Breitenstein, Transport of Hydrogen to Cylindrical Anodes in Stirred Electrolytes, J. Electrochem. Soc., 114, 349 (1967).

29. V. G. Levich, The Theory of Concentration Polarization, Acta Physicochimica, USSR, 17, 257 (1942).

30. R. F. Fleming, Compilation of Physical and Chemical Properties of Materials and Streams Encountered in the Chemical Processing Department, USAEC report HW-57386 (September 16, 1958).

31. C. O. Bennett and J. E. Meyers, Momentum, Heat and Mass Transfer, p. 509, McGraw-Hill, New York (1962).

32. W. H. McAdams, Heat Transmission, p. 358, McGraw-Hill, New York (1954).

33. C. O. Bennett and J. E. Meyers, Momentum, Heat and Mass Transfer, p. 341, McGraw-Hill, New York (1962).

34. E. R. G. Eckert, Introduction to Transfer of Heat and Mass, p. 142, McGraw-Hill (1950).

35. I. G. Knudsen and D. L. Katz, Fluid Dynamics and Heat Transfer, Engineering Institute Bulletin No. 37, p. 153, University of Michigan Press (1953).

36. J. H. Perry, Chemical Engineer's Handbook, p. 393, McGraw-Hill, New York (1950).